

## Article

# Spatial Relationship between Eclogite and Copper-Nickel Mineralization in East Kunlun, China

Yong Zhang <sup>1</sup>, Tong Pan <sup>2,\*</sup>, Aikui Zhang <sup>1,\*</sup>, Shuyue He <sup>1</sup>, Ye Qian <sup>3</sup> and Yongshan Bai <sup>4</sup><sup>1</sup> The Third Geological Exploration Institute of Qinghai Province, Xining 810029, China<sup>2</sup> Bureau of Geology and Mineral Exploration and Development of Qinghai Province, Xining 810001, China<sup>3</sup> College of Earth Sciences, Jilin University, Changchun 130061, China<sup>4</sup> Qinghai Geological Survey Institute, Xining 810012, China

\* Correspondence: pant66@163.com (T.P.); qhszyzak@163.com (A.Z.)

**Abstract:** In recent years, Cu-Ni deposits have been discovered at different localities in the Eastern part of the Kunlun orogenic belt such as Xiarihamu, Langmuri, Shitoukengde, and Wenquan. Eclogites are usually exposed in the areas associated with these deposits, thereby implying a certain coupling relationship between the Cu-Ni deposits and eclogite distribution. In this study, eclogite samples from the Xiarihamu and Langmuri areas were analyzed using petrogeochemistry, U-Pb zircon geochronology, and electron probe microanalysis (EPMA). Further, eclogite protolith properties, the formation environment, and the metallogenic mechanism were also investigated. Geochemically, eclogite is rich in MgO and FeO and low in alkali and SiO<sub>2</sub>. Its m/f ratios are 0.72 to 1.53 and Mg<sup>#</sup> values of 42 to 61. Overall, the chondrite-normalized rare-earth elements (REE) patterns showed characteristics of weak enrichment with LREE, weak negative Eu anomalies, relative enrichment of large-ion lithophile elements such as K and Rb, active incompatible element Th, the depletion of high-field strength elements Nb, Ta, Zr, and Hf, and V-shaped valleys caused by depletion in Sr, P, and Ti. These geochemical characteristics indicated that the protolith is highly differentiated Fe gabbro that formed in a continental margin type of rift environment. The EPMA analyses showed that the composition of garnet consists of almandite and grossularite, and omphacite often contains augite. Geochronological investigations showed that the peak metamorphic age of eclogite in Xiarihamu and Langmuri is  $415.6 \pm 2.7$  Ma (MSWD = 0.43, n = 16) and  $449.1 \pm 8.5$  Ma (MSWD = 0.88, n = 19), which are related to the early Paleozoic orogenic cycle and formed slightly earlier than the formation of the magmatic liquation type of Cu-Ni deposits in this area. On the basis of spatial coupling, formation age approximation, and geochemical correlation between eclogite and mafic rock masses, in combination with the previous research results of earlier work, it has been considered that the Cu-Ni ore deposits in the East Kunlun Range were formed in the post-collisional extension environment after the deep subduction of the continental crust. The ultra-high-pressure metamorphic melange formed by continental deep subduction or the enriched mantle formed by crust-mantle metasomatism was partially melted to form sulfur-rich mafic-ultramafic magmas in the post-collision extension environment. During the deep subduction of the continental crust, a large amount of crust-derived sulfur was brought into the mantle, which is the key factor for the mineralization of Cu-Ni ore in the region.

**Keywords:** eclogite; petrogeochemistry; geochronology; metallogenic mechanism; Xiarihamu; Langmuri; East Kunlun



**Citation:** Zhang, Y.; Pan, T.; Zhang, A.; He, S.; Qian, Y.; Bai, Y. Spatial Relationship between Eclogite and Copper-Nickel Mineralization in East Kunlun, China. *Minerals* **2023**, *13*, 330. <https://doi.org/10.3390/min13030330>

Received: 3 December 2022

Revised: 22 January 2023

Accepted: 23 February 2023

Published: 26 February 2023



**Copyright:** © 2023 by the authors. Licensee MDPI, Basel, Switzerland. This article is an open access article distributed under the terms and conditions of the Creative Commons Attribution (CC BY) license (<https://creativecommons.org/licenses/by/4.0/>).

## 1. Introduction

From previous works, there is a belief that magmatic liquation-type Cu-Ni deposits associated with ultrabasic rocks in China are usually formed in fault sag areas [1–3]. However, the super-large Xiarihamu Cu-Ni deposit recently discovered in East Kunlun questioned this view. This deposit is not only the largest orogenic magmatic liquation

Cu-Ni deposit in China with a nickel content of 1.05 million tons, but also one of the 20 largest Ni deposits in the world [4]. The discovery of the Xiarihamu deposit has inspired the search for Cu-Ni deposits in the orogenic environment in East Kunlun and the whole of China. Several small and medium size Cu-Ni deposits have been discovered in East Kunlun following the discovery, and great progress has been made in prospecting. For example, the Shitoukengde Cu-Ni deposit was discovered in the Wulonggou area [5,6], the Langmuri Cu-Ni deposit has been discovered in the upper reaches of the Langmuri-Gazhima area [7], and ore-bearing ultramafic rocks were also found in the Wengquan area [8,9].

It is noteworthy that eclogite outcrops have been reported all around the Cu-Ni deposits in East Kunlun. For example, sporadic eclogite outcrops of approximately 20 km have been found in the Suhaitu-Xiarihamu mining area located within the Xiarihamu Cu-Ni deposit [10–12]. In addition, irregular eclogite outcrops were also reported from the Dagele-Wulonggou area, where the Shitoukengde deposit is located [13,14]. The presence of eclogite has also been reported from Langmuri to Gazhima in the eastern segment of East Kunlun [15] and in the Wenquan area [8,16,17] (Figure 1b). The distribution characteristics of eclogites and Cu-Ni deposits indicate that there may be a coupling relationship between them.

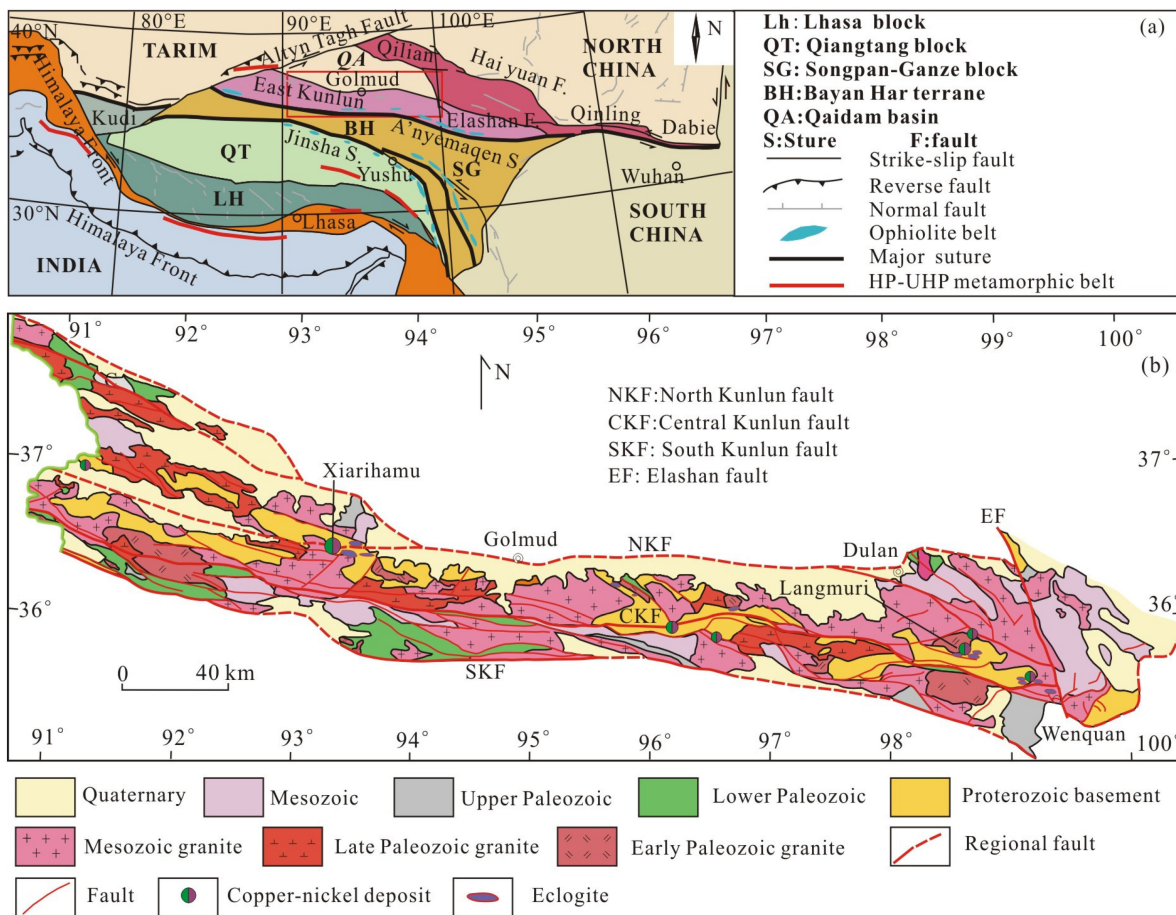


**Figure 1.** (a) Tectonic position (revised after Ma et al. [18]) and (b) geological map of East Kunlun, China.

Previous studies have either studied the plate movement based on eclogites and believed that the continental collision occurred in East Kunlun during the Early Paleozoic [10,14–17] or studied the genesis and sulfur saturation mechanism of Cu-Ni deposits according to the metallogenic characteristics. It is generally believed that crust sulfur mixing is the key factor of sulfur saturation and sulfide fusion [19–23]. However, the linkage between eclogite and Cu-Ni mineralization has only received a very scant amount of attention. As a result, many crucial questions are yet unsolved. What links the spatial dis-

tribution of eclogite and Cu-Ni deposits in East Kunlun? Have the orogenic Cu-Ni deposits formed only in a specific tectonic environment during eclogite subduction metamorphism, peak HP-UHP metamorphism, and retrograde metamorphism? Or were some molten fluids produced during eclogite prograde and retrograde metamorphism the key inducing factors for Cu-Ni sulfide melting? Could the coupling relationship between eclogite and Cu-Ni deposits in the East Kunlun area be just an accidental event?

In order to answer these questions, it is necessary to determine whether they are contemporaneous products and whether there is any petrogeochemical correlation. For this reason, we selected eclogites from Xiarihamu and Langmuri Cu-Ni mining areas in East Kunlun for petrogeochemistry, U-Pb zircon geochronology, and electron probe microanalysis (EPMA) studies. Combined with previous research results of sulfur isotopes, platinum group elements, and volatile components, a new model of sulfur addition in the subduction channel of magmatic liquation-type Cu-Ni deposits in East Kunlun was proposed. This sulfur addition model and the previously considered crustal sulfur contamination during magma emplacement [19–23] jointly led to the saturation of sulfur in this type of deposit. It provides a new idea for the metallogenic mechanism of magmatic liquation-type Cu-Ni deposits in orogenic belts.

## 2. Geologic Setting

The East Kunlun orogenic belt (EKOB) is located on the northeast edge of the Qinghai-Tibet Plateau, starting from Altun in the west to Elashan in the east, Qaidam Basin in the north, and Bayan Har in the south (Figure 1a). It is an orogenic belt that lies in the Qinghai-Tibet Plateau and is characterized by soft collision [24,25] and polycyclic composite orogeny [26,27]. It has primarily been formed by four tectonic cycles [28,29]. Pan et al. [30,31] divided the East Kunlun orogenic belt into three main zones, namely, the North East Kunlun, Middle East Kunlun, and South East Kunlun, according to the volcanic structure, sedimentary record, and type of mineralization.

In East Kunlun, the exposed strata range from the Paleoproterozoic to Cenozoic. Although the Paleoproterozoic, Mesozoic, and Cenozoic strata are the ones most widely distributed (Figure 1b), their distribution varies in different structural zones. The volcanic and pyroclastic rocks of the Ordovician, Devonian, and Triassic periods, and some remnants of the Paleoproterozoic metamorphic basement, are primarily exposed in North East Kunlun. Proterozoic middle-high metamorphic rock series, especially the Paleoproterozoic Jinshuikou rock group, is the most widely distributed formation in the region, and continental volcanic-sedimentary rocks from the Late Devonian to Early Permian are present in Middle East Kunlun. The strata of different periods are exposed in South East Kunlun. The Paleozoic strata include meso-mafic volcanic and clastic rocks. A series of foreland basin sedimentary strata, such as the Hongshuichuan Formation, Naocangjiangou Formation, and Xilikete Formation of Mesozoic, are widely exposed.

Magmatic activity in East Kunlun has been intense and frequent, and it resulted in the formation of the famous East Kunlun tectonic magmatic belt [32]. Plutonic and volcanic rocks are widely distributed. The former, ranging in age from the Neoproterozoic to Jurassic, are primarily granite in composition, with a minor amount of peridotite and gabbro. They primarily occur in the north of the central Kunlun fault and are generally distributed in the NWW-SEE direction, which is consistent overall with the direction of regional tectonic lines [33].

The East Kunlun area is an important mineral resource base in Qinghai Province. A number of iron, copper, lead, zinc, gold, silver, cobalt, tungsten, tin, and other important deposits of significant economic value have been discovered [21,22,29,34–36]. These minerals were primarily formed by the four orogenies in East Kunlun, and the magmatic liquation-type Cu-Ni deposits were primarily formed during the second orogenesis (Early Paleozoic).

### 3. Distribution Characteristics of Eclogite

Eclogites in the East Kunlun area are primarily found in Middle East Kunlun and are generally distributed in the form of groups. They are exposed from west to east in Suhaitu-Xiarihamu, Dagele-Wulonggou, Langmuri upstream-Gazhima area, and Wenquan, forming a 500 km long high-pressure metamorphic belt (Figure 1b). The distribution of eclogite generally shows that the north and south sides of the Middle East Kunlun block are obviously denser than the middle part, and the eastern part is denser than the western part. At the same time, the distribution of eclogite tends to move south gradually from west to east. Eclogite in the western part of the block is close to the side of the North East Kunlun fault, whereas the eastern part of Langmuri is primarily present close to the side of the central East Kunlun fault. The most developed and widely distributed eclogite is found in the triangle formed at the point where the central East Kunlun and Wenquan faults cross-cut. Eclogite is generally exposed as a large tectonic block, distributed in NW or near EW, running parallel to the regional tectonic direction. Eclogite blocks typically measure between 2.5 and 25 m in width and less than 50 m in length, while the largest eclogite, which can be found in Xiarihamu, is approximately 400 m long and 300 m wide.

#### 3.1. Distribution Characteristics of Eclogite from Xiarihamu

Four eclogites were identified in the Xiarihamu mining area (Figure 2a). Eclogite is primarily detected to occur at the edge of the mafic-ultramafic rock mass and shows spatial coupling with the latter. Eclogite I is located approximately 500 m to the northwest of the main ore-bearing mafic-ultramafic rock mass, with an outcrop area of approximately 0.1 km<sup>2</sup> and an exposed thickness of approximately 120 m in the borehole ZK2721. It occurs as a lenticular body in gneiss of the Paleoproterozoic Jinshuikou group. Although eclogite is not in direct contact with the ore-bearing rock mass, it is in direct contact with the host rock (pyroxenite) of the Cu-Ni ore. Pyroxene and eclogite are in intrusive contact, and pyroxenite is located at the bottom of eclogite. Eclogite II is distributed in the east-west direction, its block is approximately 550 m long and 200 m wide, and it has an area of approximately 0.1 km<sup>2</sup>. Eclogite III is nearly elliptical in shape, has an outcrop area of approximately 0.35 km<sup>2</sup>, and contains a small amount of peridotite. Eclogite IV is distributed in the east-west direction and has an outcrop area of approximately 0.1 km<sup>2</sup> [21,22,37].

#### 3.2. Distribution Characteristics of Eclogite from Langmuri

In the south of the Langmuri mining area, eclogite is primarily distributed along the Langmuri-Gazhima area. It occurs as tectonic blocks of different sizes in the Paleoproterozoic Jinshuikou group or Neoproterozoic granitic gneiss. The eclogite belt is spasmodically exposed and is approximately 18 km long and 1–3 km wide [15]. Four eclogites (Figure 2b) have been found in the Langmuri mining area, which are usually distributed around mafic-ultramafic rocks. These eclogites are mostly distributed in lenticular clusters, with a strike in the E-W directions, 10–200 m long and 3–50 m wide. Eclogite I is the largest, which is 200 m long and 50 m wide and has an outcrop area of approximately 0.1 km<sup>2</sup>.

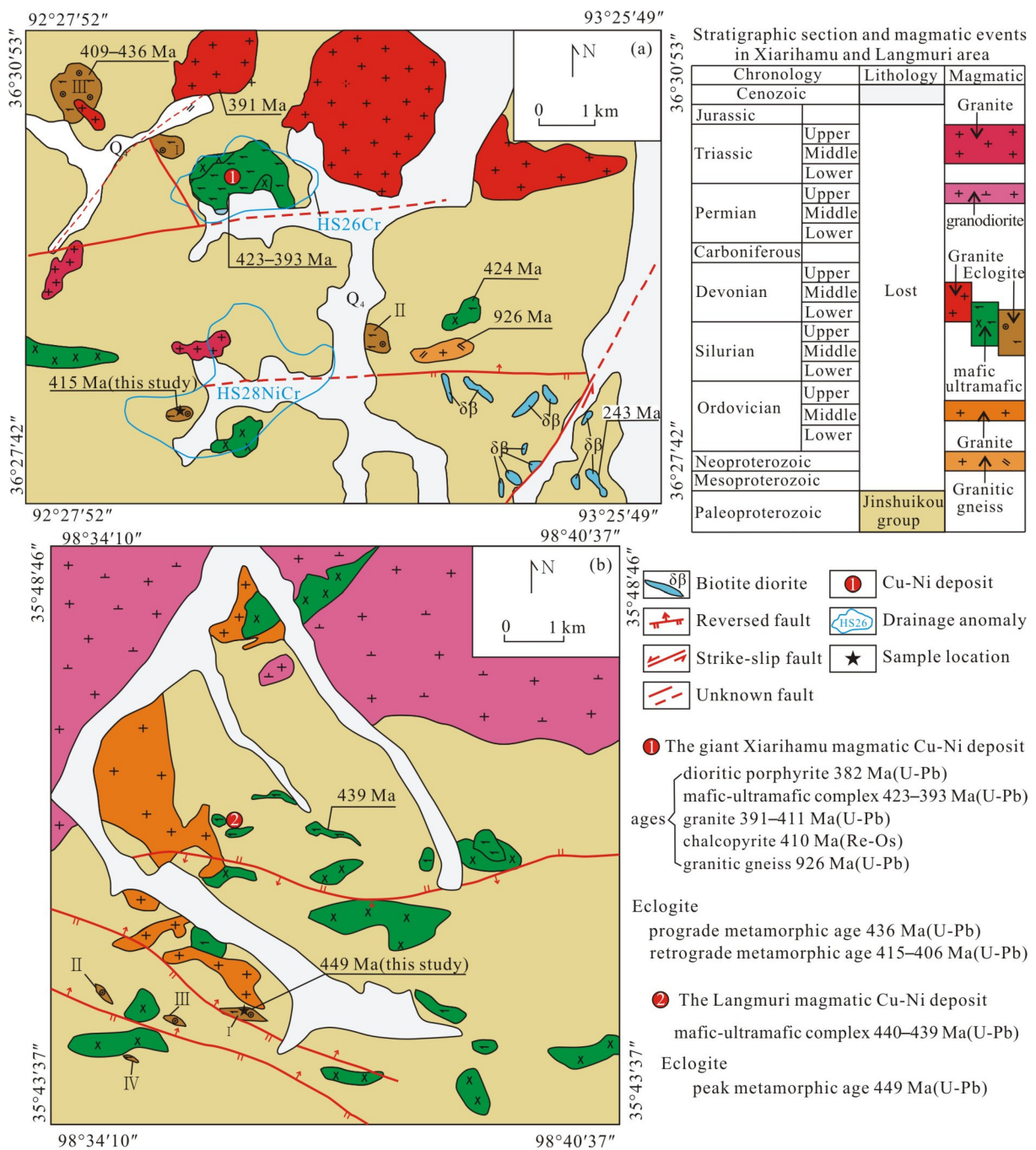


**Figure 2.** Geological maps of Xiarihamu ((a), revised after Pan [18]) and Langmuri ((b), revised after Meng [38]) Cu-Ni mining area. Geochronological data are based on references [4,10,11,19,20,23,37–39].

### 4. Sample Collection and Methodology

#### 4.1. Samples Collection

In this study, a total of 16 eclogite samples were collected as samples for petrogeochemistry, U-Pb zircon geochronology, and electron probe mineral analysis. See Table 1 for the collected information on each sample.

**Table 1.** List of samples collection on Xiarihamu and Langmuri.

Sample	Type	Weight	Area	Coordinates	Description
XRHMN1 GS1–GS5 DZ1–DZ2	U-Pb zircon Whole-rock analyses EPMA	31 kg ~1 kg ~0.5 kg	Xiarihamu	93°24′21″ E, 36°26′50″ N	Collected intact and fresh rocks, dark grayish-green in color, composed of omphacite, garnet, plagioclase, hornblende, quartz, and biotite.
LMRN1 GS6–GS10 DZ3–DZ4	U-Pb zircon Whole-rock analyses EPMA	35 kg ~1 kg ~0.5 kg	Langmuri	98°36′29″ E, 35°44′41″ N	Collected intact and fresh rocks, dark grayish-green in color, composed of omphacite, garnet, plagioclase, quartz, hornblende, and rutile.

## 4.2. Experimental Procedure

### 4.2.1. Geochemical Analyses

Major and trace element analyses were carried out at the Key Laboratory of Mineral Resources Evaluation in Northeast Asia of the Ministry of natural resources (Jilin, China). FeO was determined by acid digestion and potassium dichromate titration, while the other major elements were determined by X-ray fluorescence spectrometry (XRF), with an analytical error of less than 3% for the major elements. The trace elements were determined by inductively coupled plasma mass spectrometry (ICP-MS), with an analytical error of less than 5%.

### 4.2.2. Electron Probe Microanalysis

The electron probe analyses were conducted at the Key Laboratory of Mineralization and Resource Evaluation of the Ministry of Land and Resources, Institute of Mineral Resources, Chinese Academy of Geological Sciences. The instrument used was a JXA-8230, with an acceleration voltage of 15 kV, a current of 20 nA, and a beam spot diameter of 5 µm. Natural minerals or synthetic metals were used as standard samples per national standards. Data were corrected online using a modified ZAF correction procedure, and the selected spectral line system was a K $\alpha$  spectral line. Details of EPMA methods are described in reference [40].

### 4.2.3. U-Pb Zircon Dating

The selection of zircon for U-Pb dating was completed at the Langfang Hongxin Geological Exploration Technology Service Co., Ltd. (Langfang, China). First, the samples were washed and dried, and then they were pulverized to 80 mesh. After rough scouring, approximately 200 zircon grains with good crystalline form and transparency were manually selected using a binocular microscope. These grains were then mounted with epoxy resin on the sample target and were subsequently ground and polished until the center of the zircon grains was exposed. Finally, transmitted light, reflected light, and cathodoluminescence micrographs of the zircon grains were taken.

The U-Pb zircon dating was completed by the Beijing Yandu Zhongshi Testing Technology Co., Ltd. The zircon trace element contents determination and U-Pb isotope dating were carried out simultaneously using LA-ICP-MS, with a New Wave UP213 laser ablation system and a Bruker M90 ICP-MS. During the laser ablation process, helium was used as the carrier gas and argon was used as the compensation gas to adjust the sensitivity. The two gases were mixed by a homogenizer before entering the ICP. The resolved signals of each sample point included a 20 to 30 s blank signal and a 50 s sample signal. Zircon standard 91,500 and Plesovice were used as external standards for the isotope fractionation correction in the U-Pb isotope dating. The zircon trace element contents were quantitatively calculated using SRM610 as the multiple external standard and Si as the internal standard [41].

## 5. Results

### 5.1. Petrography

#### 5.1.1. Petrography of Eclogite from Xiarihamu

Eclogite from the Xiarihamu area is dark grayish-green to dark green in color. It has a subhedral-anhedral granular texture and a massive structure (Figure 3a–c), most of which has been converted to garnet amphibolite through retrograde metamorphism. It is primarily composed of omphacite (35%–40%), garnet (25%–30%), plagioclase (20%–25%), hornblende (10%–15%), quartz (5%–10%), and biotite (3%–5%). Omphacite is subhedral-anhedral columnar with a grain size of 0.1–2 mm. The aggregate is an irregular heap, which is locally metasomatized by calcite, and it occurs with garnet as a granular mosaic. Garnet is subhedral granular with a grain size of approximately 4 mm; it has a scattered distribution and is locally metasomatized to calcite and chlorite. Plagioclase is anhedral granular with a size range from 0.05 to 1 mm and often intersected with hornblende to form the reaction edge of garnet corona (Figure 3e), which is a retrograde metamorphic product. Hornblende is anhedral columnar, has a scattered distribution, and is generally 0.1–2 mm in size (Figure 3e,f). Quartz is anhedral granular, has a scattered distribution, and is generally 0.03–1.5 mm in size. Biotite is flaky with a diameter of 0.1–1 mm, and the aggregate is distributed in streaks and stripes (Figure 3e).

Metallic minerals primarily include pyrrhotite (1%–2%), ilmenite (0.1%–0.5%), and a small amount of chalcopyrite. Pyrrhotite is anhedral granular with a scattered distribution. It is generally 0.1 to 0.5 mm in size, but some grains are 0.5 to 1 mm, with a small contribution of grains that are 0.01 to 0.1 mm, and, rarely, 1 to 2 mm. Chalcopyrite is anhedral granular with a scattered distribution. It is generally 0.01 to 0.05 mm in size, but some grains are 0.05–0.1 mm, with a minority of them being 0.1 to 0.2 mm or, rarely, 0.2 to 1 mm. Angular metasomatic pyrrhotite has also been found locally (Figure 3f).

#### 5.1.2. Petrography of Eclogite from Langmuri

Eclogite in Langmuri is gray-green to dark green in color, and it has a subhedral-anhedral granular texture and a massive structure (Figure 3h,i), which is primarily composed of omphacite (40%–41%), garnet (35%–38%), plagioclase (5%–10%), quartz (5%–8%), hornblende (4%–7%), and rutile (3%–5%). Omphacite is subhedral-anhedral columnar with a grain size of 0.3 to 2 mm, and it has a granular mosaic structure with garnet. Garnet is subhedral granular, with a grain size of 1 to 3 mm, and is locally metasomatized to actinolite, chlorite, and other minerals. Plagioclase is anhedral granular with a grain size of 0.1 to 1 mm, often intersected with hornblende to form the reaction edge of garnet corona (Figure 3k). Quartz is anhedral granular, has a scattered distribution, and is generally 0.05 to 1 mm in size, with irregular cracks and wavy extinction. Hornblende is anhedral columnar, has a scattered distribution, and is generally 0.5 to 1.5 mm in size. Rutile occurs in the form of inclusions in garnet and pyroxene (Figure 3k).

### 5.2. Geochemistry

#### 5.2.1. Major Elements

The major element analyses for the eclogite are shown in Table 2. The Xiarihamu eclogite has SiO<sub>2</sub> ranges from 47.56 wt.% to 51.32 wt.%, with an average of 49.23 wt.%. The MgO varies only slightly from 6.31 wt.% to 6.55 wt.%, with an average of 6.37 wt.%. The FeO ranges from 9.42 wt.% to 13.55 wt.%, with an average of 11.08 wt.%. The Fe<sub>2</sub>O<sub>3</sub> ranges from 1.11 wt.% to 2.18 wt.%, with an average of 1.41 wt.%, and the m/f ratios range from 0.72 to 1.04. The Al<sub>2</sub>O<sub>3</sub> ranges from 12.48 wt.% to 13.53 wt.%, which is moderate. The Na<sub>2</sub>O ranges from 2.07 wt.% to 2.57 wt.%, the K<sub>2</sub>O ranges from 0.17 wt.% to 1.76 wt.%, and the  $\omega$  (Na<sub>2</sub>O)/ $\omega$  (K<sub>2</sub>O) ratios range from 1.27 to 14.76. In the Nb/Y-SiO<sub>2</sub> diagram (Figure 4a), all the samples are plotted in the SubAlkalBas series. In the Ta/Yb-Ce/Yb diagram (Figure 4b), the samples are primarily plotted in the calc-alkaline series. In general, the eclogite of Xiarihamu is characterized by high MgO and FeO, low alkali, and poor SiO<sub>2</sub>.

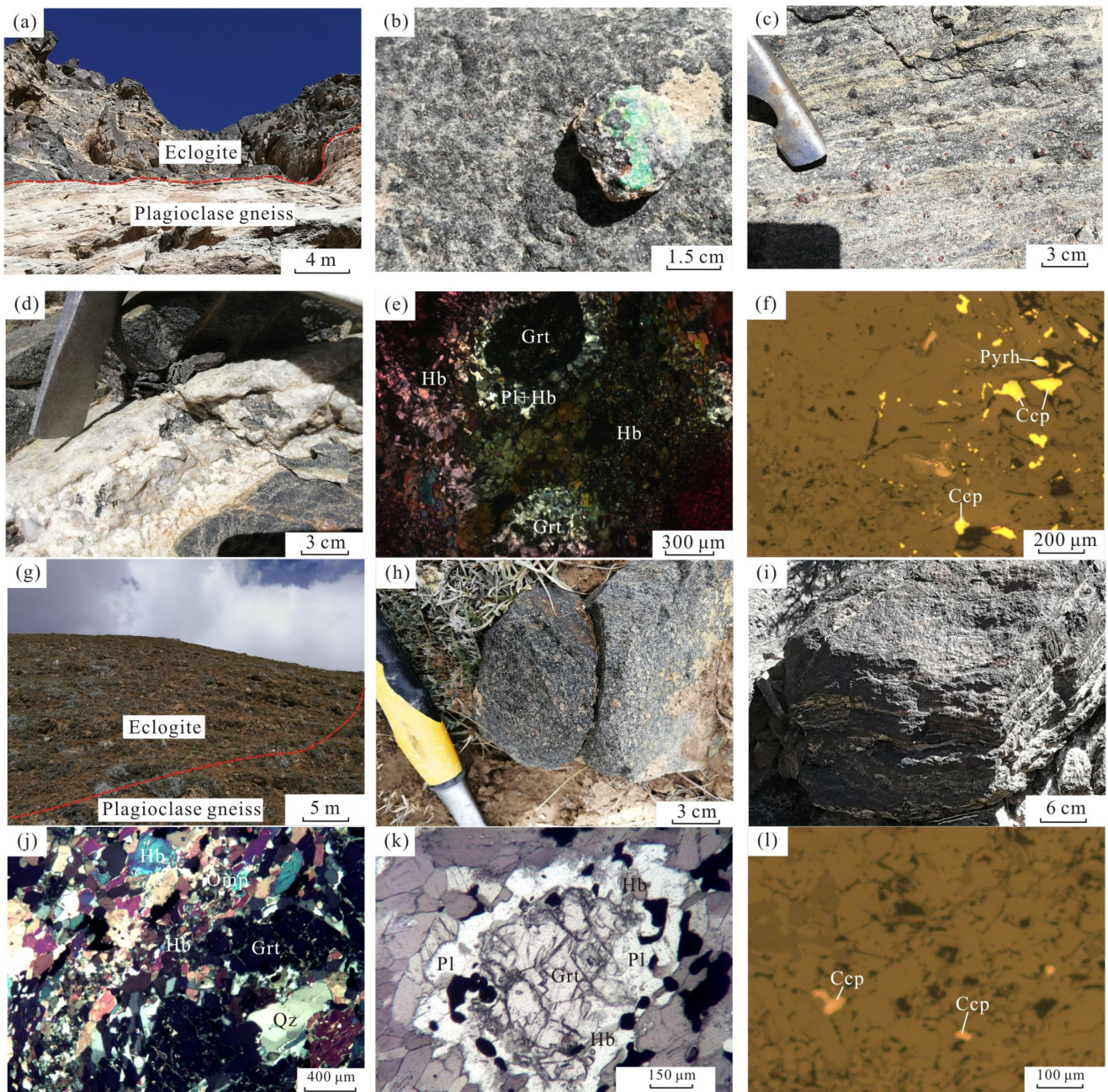


**Figure 3.** Representative photographs of the eclogites from Xiarihamu (a–f) and Langmuri areas (g–l). (a,g) Macroscopic photograph of eclogite outcrop; (b,h) photograph of eclogite and weak malachite; (c,i) stratiform eclogite; (d) quartz vein in eclogite; (e,k) post-synthetic crystals of plagioclase and amphibole at the edge of garnet; (f,l) reflected light photomicrograph showing chalcopyrite or pyrrhotite; (j) crossed polarized light photomicrograph showing mineral characteristics of eclogite. Mineral code: Grt = Garnet, Hb = Hornblende, Pl = Plagioclase, Omp = Omphacite, Qz = Quartz, Ccp = Chalcopyrite, Pyr = Pyrrhotite.

**Table 2.** Major elements (wt.%), rare earth elements (ppm), trace elements (ppm), and other parameters of the eclogite from Xiarihamu and Langmuri areas.

Sample	GS1	GS2	GS3	GS4	GS5	GS6	GS7	GS8	GS9	GS10
area	Xiarihamu					Langmuri				
SiO <sub>2</sub>	47.56	50.82	47.57	48.86	51.32	50.79	52.16	52.32	49.63	50.54
Al <sub>2</sub> O <sub>3</sub>	12.48	12.70	13.53	13.21	12.82	11.79	12.81	11.18	11.66	12.37
Fe <sub>2</sub> O <sub>3</sub>	1.30	1.11	2.18	1.89	1.41	0.24	0.1	0.13	0.24	0.1
FeO	11.50	9.42	13.55	11.12	9.83	12.31	11.83	12.39	12.83	12.34
MgO	6.32	6.32	6.35	6.55	6.31	10.35	9.64	10.17	10.87	10.31
CaO	13.50	10.44	10.92	12.38	11.01	11.12	11.03	10.86	10.52	10.73
Na <sub>2</sub> O	2.07	2.24	2.51	2.57	2.35	1.26	1.09	1.09	0.95	1.11
K <sub>2</sub> O	0.90	1.76	0.17	0.42	1.07	0.21	0.15	0.15	0.17	0.25
TiO <sub>2</sub>	1.26	1.12	1.59	1.26	1.21	1.01	0.76	0.91	0.95	0.93
P <sub>2</sub> O <sub>5</sub>	0.10	0.12	0.12	0.09	0.12	0.07	0.22	0.06	0.12	0.11
MnO	0.26	0.46	0.31	0.21	0.37	0.21	0.21	0.22	0.33	0.32
LOI	2.67	3.24	1.61	2.18	2.28	0.37	0.29	0.49	0.51	0.48
Total	99.92	99.75	100.41	100.74	100.1	99.73	100.29	99.97	98.78	99.59
m/f	0.87	1.04	0.72	0.90	0.98	1.46	1.38	1.53	1.48	1.43
Mg <sup>#</sup>	47.1	51.7	41.9	47.3	50.0	59.32	58.80	61.24	60.21	59.00
La	7.7	19.9	5.8	5.8	14.3	3.85	9.32	4.09	4.80	5.45
Ce	18.4	44.7	14.9	14.4	32.7	7.65	17.99	15.26	11.32	10.64
Pr	2.34	5.22	2.16	2.02	3.92	1.50	2.78	1.54	1.72	1.87
Nd	10.7	20.7	10.6	9.90	16.5	7.69	12.73	8.19	9.01	9.26
Sm	3.27	4.85	3.78	3.07	4.29	2.54	3.34	2.61	2.70	2.80
Eu	1.07	1.41	1.31	1.15	1.28	0.81	1.11	0.84	0.86	0.92
Gd	4.57	5.79	5.63	4.74	5.46	2.81	3.88	2.97	3.00	3.15
Tb	0.87	1.07	1.12	0.84	0.99	0.65	0.74	0.67	0.67	0.68
Dy	5.89	6.70	8.10	5.68	6.45	3.95	4.41	4.25	4.10	4.12
Ho	1.34	1.45	1.83	1.29	1.42	0.98	1.04	1.06	1.02	1.00
Er	3.94	4.25	5.52	3.71	4.15	2.73	2.84	3.07	2.81	2.79
Tm	0.56	0.62	0.87	0.54	0.61	0.45	0.45	0.49	0.45	0.46
Yb	3.77	3.95	5.68	3.48	3.99	2.83	2.82	3.11	2.77	2.82
Lu	0.57	0.60	0.88	0.55	0.62	0.46	0.46	0.51	0.46	0.47
Y	33.4	35.4	44.6	31.8	35.0	22.97	25.04	25.21	23.44	24.10
ΣREE	64.99	121.21	68.18	57.17	96.68	38.90	63.91	48.66	45.69	46.43
LREE/HREE	2.02	3.96	1.30	1.74	3.08	1.62	2.84	2.02	1.99	2.00
(La/Yb) <sub>N</sub>	1.38	3.40	0.69	1.13	2.42	0.92	2.23	0.89	1.17	1.31
δEu	0.85	0.81	0.87	0.92	0.81	0.92	0.94	0.92	0.92	0.94
δCe	1.01	1.01	0.99	0.99	1.01	0.75	0.82	1.42	0.92	0.78
Rb	27.1	59.1	6.1	11.4	35.7	4.49	7.61	3.91	8.20	6.92
Ba	392	1286	55	203	909	20.29	28.81	17.59	27.91	33.78
Th	1.69	6.47	0.91	0.79	4.36	0.66	1.32	0.66	0.98	0.97
Ta	0.49	0.71	0.45	0.39	0.60	0.51	0.53	0.51	0.51	0.51
Nb	7.10	10.7	7.40	6.40	8.98	0.51	0.75	0.53	0.56	0.63
Hf	2.70	3.70	3.00	2.30	3.20	10.85	10.43	10.86	10.86	10.68
Zr	89.0	117	93.0	71.0	101.8	51.93	45.15	52.80	55.94	52.33
Sr	172.0	190.0	122.0	230	191.6	110.00	103.95	119.38	124.47	117.16
P	436	524	524	393	524	306.63	962.18	260.16	349.26	480.33
Cr	110	140	90	110	116	312.64	342.09	350.21	292.28	309.25
Cs	2.91	4.60	1.17	1.73	2.99	0.18	0.43	0.18	0.31	0.30
Sc	43.3	32.7	50.9	44.0	37.6	51.38	52.63	56.25	46.54	49.85
V	472	382	596	478	430	293.73	288.04	293.60	267.88	282.30
Ga	17.0	19.7	17.0	18.9	18.1	0.53	1.06	0.53	0.80	3.27

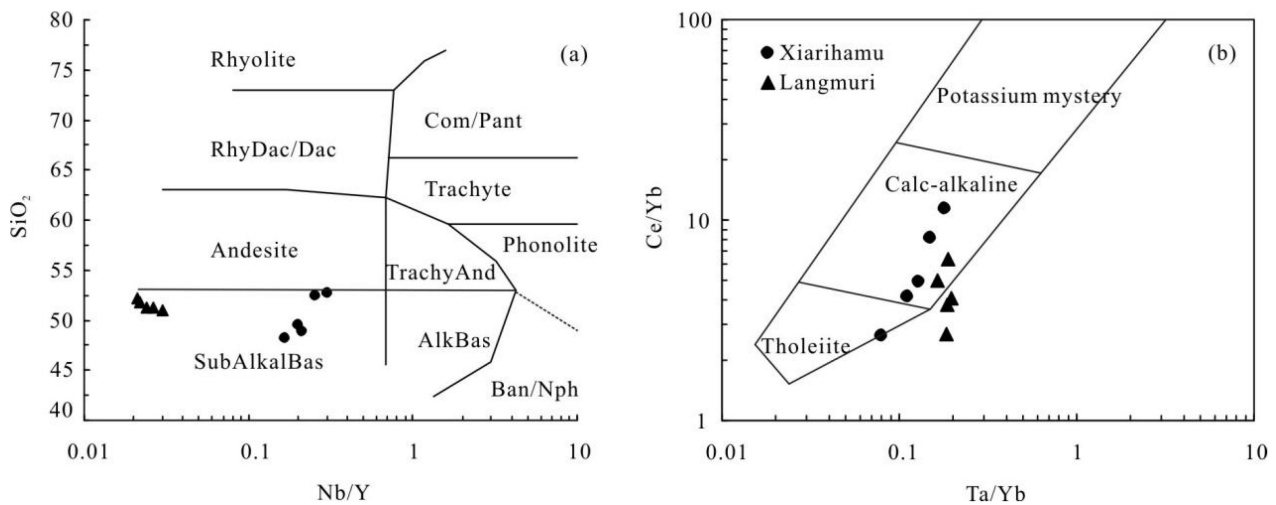


**Figure 4.** (a) Nb/Y-SiO<sub>2</sub> (after Winchester and Floyd [42]) and (b) Ta/Yb-Ce/Yb (after Muller and Groves [43]) diagram of the eclogite.

The eclogite from the Langmuri area has SiO<sub>2</sub> ranging from 49.63 wt.% to 52.32 wt.%, with an average of 51.09 wt.%. The MgO ranges from 9.64 wt.% to 10.87 wt.%, with an average of 10.27 wt.%, and is rich in Mg. The FeO ranges from 11.83 wt.% to 12.83 wt.%, with an average of 12.34 wt.%. The Fe<sub>2</sub>O<sub>3</sub> ranges from 0.10 wt.% to 0.24 wt.%, with an average of 0.16 wt.%, and the m/f ratios range from 1.42 to 1.45. The Al<sub>2</sub>O<sub>3</sub> ranges from 11.18 wt.% to 12.8 wt.1%, which is moderate. The Na<sub>2</sub>O ranges from 0.95 wt.% to 1.26 wt.%, the K<sub>2</sub>O ranges from 0.15 wt.% to 0.25 wt.%, and the  $\omega(\text{Na}_2\text{O})/\omega(\text{K}_2\text{O})$  ratios range from 4.44 to 7.27. In the Nb/Y-SiO<sub>2</sub> diagram, all the samples (Figure 4a) are plotted in the SubAlkalBas series. In the Ta/Yb-Ce/Yb diagram (Figure 4b), the samples are primarily plotted in the calc-alkaline series and at its edges. The eclogites of Langmuri and Xiarihamu have similar major element characteristics and also have high MgO and FeO, low alkali, and poor SiO<sub>2</sub>.

### 5.2.2. Rare Earth Elements (REEs)

The total rare earth elements ( $\Sigma\text{REE}$ ) of the eclogite from the Xiarihamu area ranges from 57.17 to 121.21 ppm, and its LREE/HREE ratio ranges from 1.30 to 3.96, indicating that the light and heavy REE (LREE and HREE) are weakly differentiated. The  $(\text{La}/\text{Yb})_{\text{N}}$  value ranges from 0.69 to 3.40, and all of the samples except GS3 are weakly enriched in LREE.  $\delta\text{Eu}$  ranges from 0.81 to 0.92, indicating negative Eu anomalies, which is related to the large amount of plagioclase in the eclogite.  $\delta\text{Ce}$  ranges from 0.99 to 1.01, and the Ce anomaly is not obvious. The chondrite-normalized REE distribution patterns for all of the samples except sample GS3 exhibit rightward inclination, indicating LREE enrichment (Figure 5a). The inclinations of samples GS2 and GS5 are greater, indicating greater LREE enrichments, which are closer to the inclination of the distribution pattern of the crust. In addition, the inclination of sample GS3 is leftward, and overall, it is similar to that of E-MORB.

The REE sum ( $\Sigma\text{REE}$ ) of the eclogite in Langmuri ranges from 38.90 to 63.91 ppm, and the LREE/HREE ratio ranges from 1.62 to 2.84. The  $(\text{La}/\text{Yb})_{\text{N}}$  value ranges from 0.89 to 2.23, and all of the samples are weakly LREE enriched.  $\delta\text{Eu}$  ranges from 0.92 to 0.94, indicating negative Eu anomalies, which is related to the large amount of plagioclase in the eclogite.  $\delta\text{Ce}$  ranges from 0.75 to 1.42, and all of the samples except GS8 show clear negative anomalies, which may indicate that the rocks underwent a strong reduction environment or were carried in by Marine sediments during the formation process. The chondrite-normalized REE distribution patterns are relatively gentle, and overall, they are similar to that of E-MORB (Figure 5a). In addition, sample GS7 exhibits LREE enrichment, and overall, it is similar to that of the lower crust.

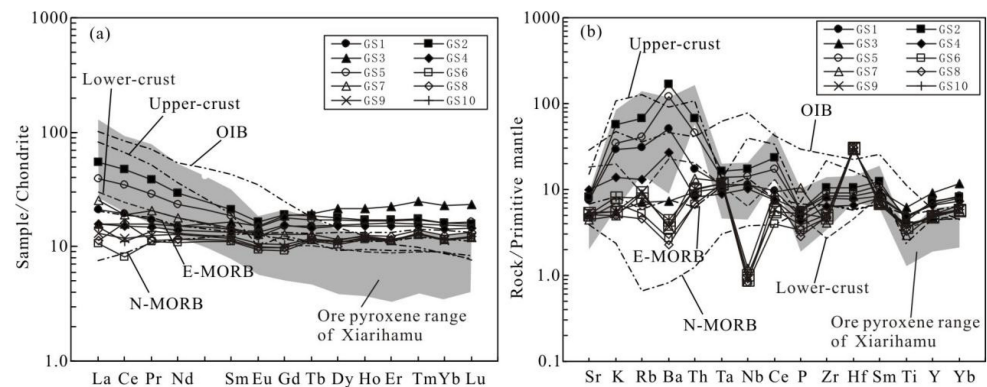


**Figure 5.** Chondrite-normalized REE distribution pattern ((a), normalization values after Taylor and McLennan [44]) and trace element spider diagram ((b), normalization, N-MORB, and E-MORB values after Sun and McDonough [45]; upper and lower crust values after Taylor and McLennan [44,46]; ore pyroxene values after Pan et al. [22]) of the eclogite in East Kunlun.

### 5.2.3. Trace Elements

As compared to the basite investigated by Turekian and Wedepohl [47], the eclogite analyzed in Xiarihamu is rich in Rb, Ba, Tm, Hf, Sb, Sc, and Dy; poor in Sr, Yb, Nb, La, Cr, and Nd; and similar in terms of the other elements. As can be seen from the primitive mantle normalized trace element spider diagram (Figure 5b), the eclogite falls between the compositions of E-MORB and the upper crust. Specifically, the eclogite is relatively rich in large-ion lithophile elements (LILEs) such as K, Rb, and Ba and the mobile-incompatible element Th. However, the composition of each element is different, especially Ba, which has a 10-fold difference between the highest and the lowest values. The high-field-strength elements (HFSEs) Nb, Ta, and Zr, Hf are relatively depleted, while Sr, P, and Ti are characterized by V-shaped valleys (depletions), which are similar to the patterns of E-MORB basalt. Based on the characteristics of the REEs, the eclogite is generally considered to have mantle-derived characteristics and to have been contaminated by crustal materials.

Compared to the basite investigated by Tuekian and Wedepohl [47], the eclogite analyzed in Langmuri is rich in Rb, Hf, and Sc, poor in Ba, Th, Nb, Zr, Sr, Cs, and Ga, and similar in terms of the other elements. As can be seen from the primitive mantle normalized trace element spider diagram, the eclogite is relatively rich in the mobile-incompatible element Th and high-field-strength elements Ta and Hf, while Ba, Nb, P, and Ti are characterized by V-shaped valleys (depletions) (Figure 5b), which are similar to the patterns of E-MORB basalt. Based on the characteristics of the REEs, the eclogite in Langmuri is generally considered to have mantle-derived characteristics and a small amount of crust-derived materials may have been introduced.

### 5.3. Mineral Chemistry

The EPMA results are shown in Table 3. The garnet of Xiarihamu eclogite is primarily composed of almandine and grossularite, with a small amount of andradite and pyrope, with the composition of  $\text{Alm}_{(59-62)}\text{And}_{(5.2-7.3)}\text{Gross}_{(26-32)}\text{Pyrope}_{(2.4-6.2)}$ . The omphacite is primarily augite (wollastonite, enstatite and ferrosilite) and jadeite, with a small amount of aegirine, with the composition of  $\text{WFe}_{(60-66)}\text{Jd}_{(24-31)}\text{Ae}_{(3-16)}$ , and the omphacite has generally been retrograded to diopside. The plagioclase is primarily andesine and labradorite, with the composition of  $\text{An}_{(34-64)}\text{Ab}_{(36-66)}\text{Or}_{(0.1-0.5)}$ . The garnet of Langmuri eclogite is primarily composed of almandine, grossularite, and pyrope, with a small amount of andradite, and its main component is  $\text{Alm}_{(56-59)}\text{And}_{(1.1-3.1)}\text{Gross}_{(21-23)}\text{Pyrope}_{(16-17)}$ . The omphacite is primarily augite (wollastonite, enstatite, and ferrosilite) and jadeite, with the composition of  $\text{WFe}_{(59-64)}\text{Jd}_{(36-41)}$ . The plagioclase is primarily oligoclase and andesine, with the composition of  $\text{An}_{(23-35)}\text{Ab}_{(64-76)}\text{Or}_{(0.3-0.5)}$ . The samples fall into the type-C

eclogite area on the Alm + Spess–Pyrope–Gross diagram for garnet (Figure 6a), and the samples fall into the omphacite area on the WEF–Jd–Ae diagram for omphacite (Figure 6b). In the Mg/(Mg + Fe<sup>2+</sup> + Mn) vs. Ca diagram of garnet, the samples of Xiarihamu are plotted in the glaucophane–schist eclogite facies, and the samples of Langmuri are plotted in the amphibolite eclogite facies (Figure 6c), all of which are typical crustal metamorphic eclogites [48].

Table 3. Electron probe analysis results (wt.%) for the eclogite samples in Xiarihamu and Langmuri.

No	SiO <sub>2</sub>	TiO <sub>2</sub>	Al <sub>2</sub> O <sub>3</sub>	FeO	MnO	MgO	Cr <sub>2</sub> O <sub>3</sub>	CaO	Na <sub>2</sub> O	K <sub>2</sub> O	P <sub>2</sub> O <sub>5</sub>	V <sub>2</sub> O <sub>3</sub>	Total	Property
Xiarihamu														
1	36.67	0.08	20.44	30.22	0.10	1.46	0.04	11.63	0.01	0.01	0.00	0.00	100.64	Garnet
2	37.12	0.04	20.23	30.22	0.16	1.31	0.03	11.51	0.09	0.00	0.05	0.04	100.79	Garnet
3	37.34	0.05	20.29	28.44	0.38	0.60	0.02	13.28	0.00	0.00	0.06	0.02	100.46	Garnet
4	36.74	0.05	20.04	29.60	0.11	1.58	0.03	12.08	0.05	0.00	0.03	0.02	100.33	Garnet
5	36.37	0.08	20.45	29.72	0.24	1.07	0.00	11.93	0.02	0.00	0.00	0.02	99.89	Garnet
6	55.47	0.07	7.38	5.54	0.02	10.48	0.02	15.91	4.92	0.02	0.01	0.02	99.86	Omphacite
7*	54.69	0.14	7.80	5.33	0.06	9.98	0.03	15.80	5.30	0.00	/	/	99.13	Omphacite
8*	53.99	0.16	8.10	5.09	0.02	10.10	0.06	15.94	5.69	0.01	/	/	99.16	Omphacite
9	51.34	0.00	0.22	11.56	0.02	10.55	0.03	23.93	0.21	0.00	0.03	0.03	97.91	Diopside
10	54.06	0.11	1.14	0.66	0.17	16.50	0.00	25.65	0.24	0.01	0.01	0.86	99.43	Diopside
11	53.19	0.02	30.27	0.20	0.01	0.00	0.00	12.45	3.86	0.02	0.00	0.00	100.01	Plagioclase
12	53.55	0.00	29.96	0.10	0.00	0.01	0.00	11.98	4.11	0.02	0.00	0.02	99.75	Plagioclase
13	60.96	0.04	24.98	0.36	0.02	0.01	0.00	6.61	7.00	0.04	0.00	0.00	100.02	Plagioclase
14	55.36	0.00	27.33	0.20	0.05	0.00	0.03	11.77	4.74	0.06	0.00	0.04	99.58	Plagioclase
15	59.05	0.02	24.96	0.10	0.02	0.00	0.00	8.08	7.01	0.08	0.01	0.01	99.34	Plagioclase
Langmuri														
16	38.22	0.10	20.95	27.16	0.55	4.34	0.00	8.47	0.02	0.00	0.01	0.07	99.89	Garnet
17	37.47	0.11	21.30	27.73	0.62	4.54	0.03	8.62	0.03	0.00	0.00	0.01	100.46	Garnet
18	37.20	0.07	21.75	27.96	0.63	4.20	0.00	8.54	0.02	0.01	0.01	0.00	100.39	Garnet
19	37.58	0.07	21.56	26.97	0.50	4.47	0.00	9.29	0.05	0.00	0.00	0.00	100.49	Garnet
20	37.02	0.13	21.81	27.36	0.62	4.47	0.00	8.56	0.04	0.00	0.00	0.02	100.03	Garnet
21	55.99	0.21	11.30	6.23	0.03	7.87	0.03	12.63	5.40	0.01	0.00	0.02	99.72	Omphacite
22	57.23	0.15	10.91	6.12	0.06	7.05	0.01	12.42	5.95	0.00	0.05	0.01	99.96	Omphacite
23	56.34	0.16	10.94	6.28	0.05	7.41	0.02	12.48	5.75	0.01	0.01	0.00	99.45	Omphacite
24	56.43	0.12	10.53	6.13	0.02	7.21	0.03	12.83	5.71	0.00	0.00	0.00	99.01	Omphacite
25	55.88	0.18	10.81	6.43	0.06	7.15	0.02	12.91	5.94	0.00	0.03	0.15	99.56	Omphacite
26	61.86	0.01	24.71	0.12	0.00	0.00	0.00	5.87	7.44	0.05	0.00	0.00	100.06	Plagioclase
27	60.65	0.00	25.48	0.18	0.02	0.00	0.03	6.85	6.91	0.07	0.02	0.00	100.21	Plagioclase
28	64.65	0.00	23.60	0.17	0.00	0.00	0.01	4.48	8.10	0.06	0.00	0.00	101.06	Plagioclase

Note: 7\* and 8\* data after Qi et al. [10].

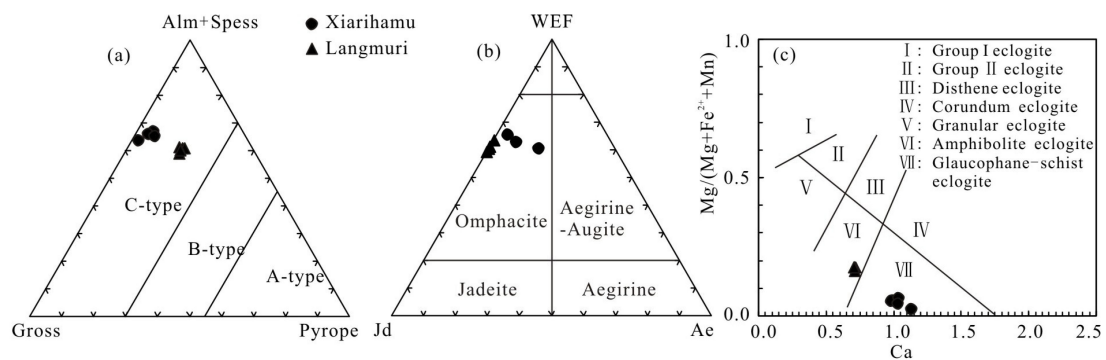


Figure 6. Composition diagram. Alm + Spess–Pyrope–Gross diagram of garnet ((a), Coleman et al. [49]), WEF–Jd–Ae diagram of omphacite ((b), Qi et al. [10]) and Mg/(Mg + Fe<sup>2+</sup> + Mn)–Ca diagram of garnet, ((c), Cong and Zhang [48]) from the eclogites in Xiarihamu and Langmuri.

#### 5.4. U-Pb Zircon Age

From the cathodoluminescence images (Figure 7e,f), it can be seen that the characteristics of Xiarihamu and Langmuri eclogite zircons are essentially the same, and most of them are irregular in shape, semi-euhedral crystals, and transparent to translucent. They mostly have a long columnar and granular morphology, with a length (along the long axis) of 60 to 180  $\mu\text{m}$ , a width (along the short axis) of 30 to 100  $\mu\text{m}$ , and an aspect ratio of 1 to 2. The zircons usually have circular edges and multi-stage growth characteristics. Zircons with irregular shapes and proliferative edges (such as the zircons at measuring points 6, 7, 8, 15, 28, and 30 in Xiarihamu and the zircons at measuring points 1, 6, 8, 9, 13, 20, 22, and 30 in Langmuri) are common, and some of the zircons remain with small debris (such as the zircons at measuring points 3, 9, 15, and 18 in Xiarihamu). The oscillatory zoning of zircon is usually faint, and most of them have the characteristics of fan zoning, which is consistent with the characteristics that metamorphic zircons often retain due to multi-stage growth regions and complex internal textures [50]. This differs from the clear oscillatory zoning texture often possessed by magmatic zircons [41,50–52].

The measured zircons of Xiarihamu contain 6–534 ppm U and 0–349 ppm Th and 0–89 ppm Pb. The U and Th contents are not high and have a large variation range. The Th/U ratios are between 0 and 1.16 and are less than 0.10 for the majority of the zircons. The measured zircons of Langmuri contain 341–30,771 ppm U, 0–2291 ppm Th, and 38–1910 ppm Pb. The U and Th contents are relatively high and have a large variation range. The Th/U ratios are between 0 and 1.03 and are less than 0.10 for most of the zircons. The Th/U ratios of greater than 0.10 are often used as an indicator for distinguishing magmatic zircons from metamorphic zircons (Belousova et al. [53]). The Th/U ratios of the Xiarihamu and Langmuri eclogite zircons indicate that they are metamorphic in origin.

The LA-ICP-MS U-Pb zircon dates of the eclogite are shown in Table S1. The  $^{206}\text{Pb}/^{238}\text{U}$  dates of the 50 measuring points of zircon from the Xiarihamu area range from 1885 to 111 Ma. From the harmonic curve (Figure 7a) and the age histogram (Figure 7c), it can be seen that the measuring points are primarily distributed in two ranges, i.e., 440 to 400 Ma, and 260 to 240 Ma. In particular, the maximum number of measuring points, which is 23, occurs in the range of 430 to 400 Ma, accounting for 46% of the total frequency. These are used as the ages of the peak metamorphism stage of the eclogite. The weighted age of the metamorphic zircons (at measuring points 2, 3, 6, 8, 20, 25, 27, 29, 31, 35, 37–39, 41, 42, and 47) has a high concordance, and a Th/U ratio of less than 0.1 in this area was calculated. The peak metamorphic age of the eclogite is  $415.6 \pm 2.7$  Ma (MSWD = 0.43,  $n = 16$ ) (Figure 7a). Based on the retrograde metamorphic age of 409 Ma for eclogite III in Xiarihamu reported by Zhang et al. [11], we speculate that the eclogite has a retrograde metamorphic age of 415 to 400 Ma.

The peak age range between 260 and 240 Ma in Xiarihamu may be the response to the Triassic magmatic activity. The single-point date of 886 Ma may represent the formation age of the eclogite's protolith. Zhang et al. [11] conducted U-Pb zircon dating of eclogite rock mass III and concluded that the crystallization age of the protolith was 806 to 701 Ma, which is relatively close to the age obtained during this study. The eclogite occurs in the Paleoproterozoic Jinshuikou group complex, which is generally considered to be the metamorphic basement of the East Kunlun orogenic belt [54], with a formation age of no later than 1300 Ma [55,56]. Therefore, the several measuring points larger than 1302 Ma obtained in this study may reflect zircons from the Jinshuikou group complex, which were captured during the prograde and retrograde metamorphism of the eclogite. Some zircon analyses show magmatic zircon characteristics, especially at points 33, 36 and 50 with U/Th ratios greater than 1. These zircons are concentrated in Proterozoic or Early Triassic, which may be residual magmatic zircons of Jinshuikou group, or magmatic zircons brought in by Triassic magmatic activity.

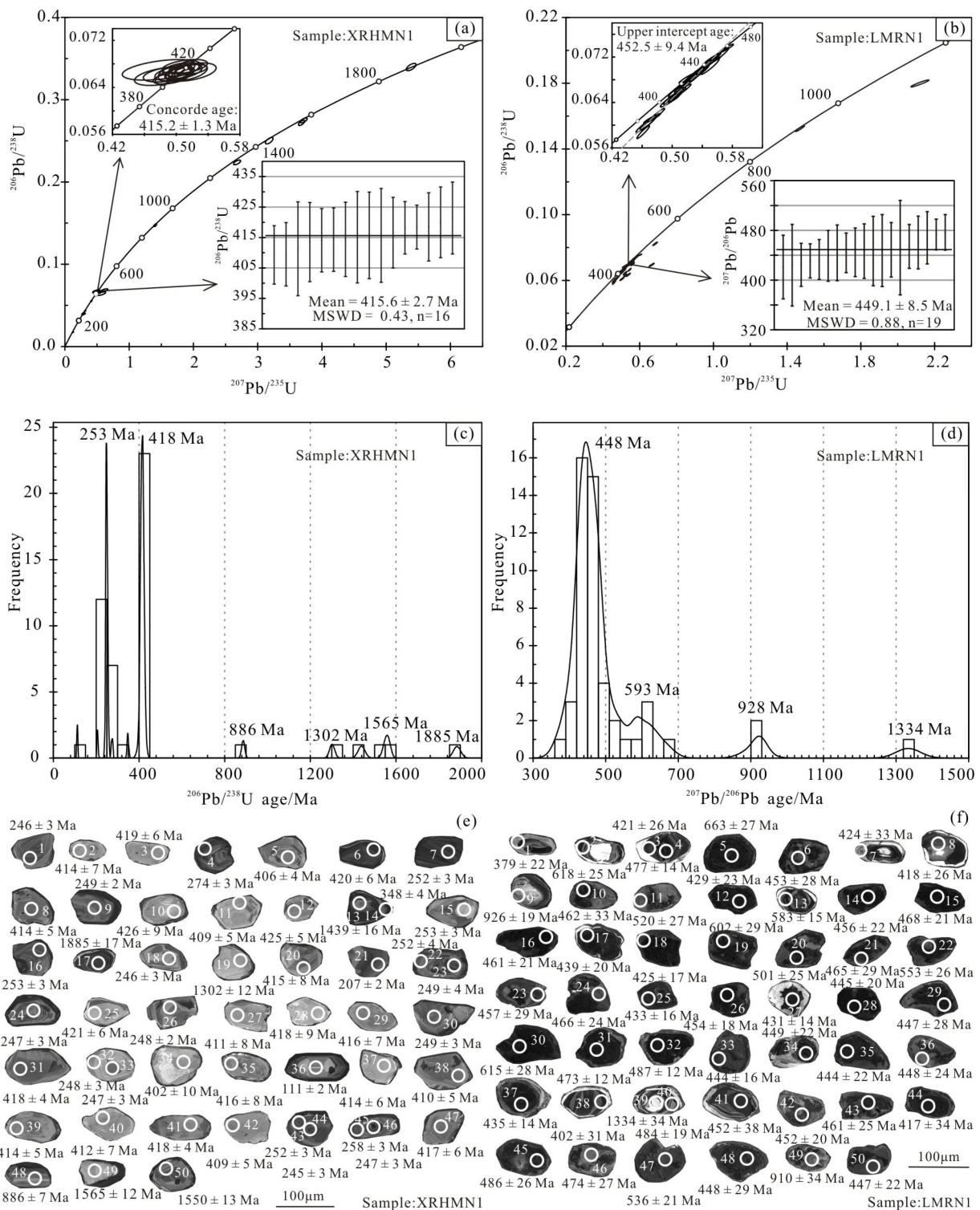


**Figure 7.** Concordia diagrams (a,b), histogram (c,d), and CL (e,f) images of zircons from the eclogite in Xiarihamu (a,c,e) and Langmuri (b,d,f) area, East Kunlun.

The  $^{206}\text{Pb}/^{238}\text{U}$  dates of the 50 measuring points of Langmuri range from 1066 to 368 Ma. From the harmonic curve (Figure 7b), it can be seen that Pb is slightly lost, and there is an inconsistent line, the age of which is  $452.5 \pm 9.4$  Ma at the upper intersection. In the case of slight loss of Pb, the upper intersection of the concordia curve represents the age of rock formation, the  $^{206}\text{Pb}/^{238}\text{U}$  age is generally younger, and the  $^{207}\text{Pb}/^{206}\text{Pb}$  age is

closer to the age of the upper intersection [57–60]. Therefore, the  $^{207}\text{Pb}/^{206}\text{Pb}$  ages were used to discuss the metamorphic age of Langmuri eclogite.

The  $^{207}\text{Pb}/^{206}\text{Pb}$  dates range from 1334 to 379 Ma and are concentrated between 480 and 420 Ma (Figure 7d). The  $^{207}\text{Pb}/^{206}\text{Pb}$  dates range from 1334 to 379 Ma and are concentrated in the range of 480 to 420 Ma (Figure 7d), which are 31 measuring points, accounting for 62% of the total frequency. These are used as the ages of the peak metamorphism stage of the eclogite. The weighted age of the metamorphic zircons (at measuring points 3, 4, 7, 15–18, 25–29, 31, 33–35, 41, 48, and 50) with a Th/U ratio of less than 0.1 in this area was calculated. The peak metamorphic age of the eclogite is  $449.1 \pm 8.5$  Ma (MSWD = 0.88,  $n = 19$ ) (Figure 7b). It is completely consistent with the upper intersection age within the error range, and it can essentially be determined that the peak metamorphic age of eclogite is from Late Ordovician to Early Silurian in Langmuri. The two older dates (910 Ma and 926 Ma) may represent the formation age of the eclogite's protolith. Some zircons from Langmuri also show the characteristics of magmatic zircons. For example, the date of the 59 measuring points is 910 Ma, which may be residual magmatic zircon of eclogite protolith.

## 6. Discussion

### 6.1. Reconstruction of the Eclogite Protolith

It has been shown that the migration of elements in eclogite is limited during complex prograde and retrograde metamorphic processes. In particular, the contents of major and REEs suffered very little variation during the eclogite facies metamorphism [61,62]. Moreover, studies of eclogite in the North Qinling Mountains have also shown that REEs and HSFES did not migrate notably during the prograde and retrograde metamorphism of eclogite [17,63,64]. Therefore, it is possible to investigate the geochemical characteristics of the protolith using concentrations of the stable elements (major elements, REEs, and HSFES) in eclogite.

The  $\text{Mg}^\#$  values of eclogite in Xiarihamu and Langmuri are 47.1–51.7 and 59–61.2, respectively. Because both value ranges are greater than 40, this indicates that the rocks have the characteristics of mantle-derived components [65], but the value is smaller than that of the original basaltic magma (68 to 75). Thus, the protolith of eclogite was not the product of the crystallization of the original basaltic magma [17,66]. There is much quartz in eclogite in Xiarihamu and Langmuri (Figure 3d,j), as in eclogite from Wenquan in East Kunlun and Maowu in Dabieshan, indicating that the protolith may have been a highly differentiated layered basite [62]. In addition, these rocks were found in Xiariham and Langmuri (Figure 3c,i). It has been shown that the protolith of many HP-UHP metamorphic eclogites is Fe-Ti-bearing gabbro [11,67,68]. Eclogite in Xiarihamu and Langmuri has  $\text{SiO}_2$  contents of 47.56 wt.% to 52.32 wt.% and m/f ratios of 0.72 to 1.53, so it seems to have been formed mainly from Fe basite. In the Nb/Y-SiO<sub>2</sub> diagram (Figure 4a), the samples are primarily plotted in the field of SubAlkalBas series. In the Ta/Yb-Ce/Yb diagram (Figure 4b), the samples are primarily plotted in the field of the calc-alkaline series. Based on this, we assume that the protoliths of eclogite in Xiarihamu and Langmuri are calc-alkaline Fe-bearing gabbro.

### 6.2. Formation Environment of the Eclogite

The Early Neoproterozoic (~1 Ga) period includes the strongest Precambrian tectonic assembly event in East Kunlun [69,70], which is synchronous with the formation of the Rodinia supercontinent on a global scale [71]. This tectonic-thermal event caused a strong, deep ductile shear flow structure and extensive anatexis in the basement rock series of the East Kunlun area [16,70,72]. In the Late Neoproterozoic, the Rodinia supercontinent was broken into several subcontinental blocks due to rifting, with a formation age of 820 to 800 Ma in China and a full-scale breakup that occurred at 700 Ma [73,74]. Ren et al. [75] studied gabbro in the Nuomuhong area of the eastern section of East Kunlun and concluded that there may have been a breakup event at  $796 \pm 41$  Ma in the eastern section of East Kunlun, which corresponds to the breakup of the Rodinia supercontinent.

This period is very close to the formation age of the eclogite protolith predicted in this study. The formation and evolution stage of the trench-arc-basin system occurred more than 550 to 460 Ma [76,77], and numerous studies have investigated the opening, expansion, and disappearance of the Tethys Ocean in East Kunlun during that period. Before the Early Cambrian (>550 Ma), the Tethys Ocean in East Kunlun opened and expanded [69,76]. The subduction of the Central Kunlun Ocean Basin may have occurred at 515 Ma [78], whereas the end of this subduction and the start of the collision were marked by the appearance of the Late Ordovician Tumuleke glaucophane schist and its accompanying gabbro (with an Ar-Ar age of  $445 \pm 2$  Ma) [33,79]. The continental crust type eclogite appearing at 436 to 431 Ma represents the closure of the Central Kunlun Ocean Basin [17]. Beginning in the Early Devonian (~413 Ma), the East Kunlun area shifted from a collision-extrusion environment to a post-collisional extensional environment [33,79,80].

The formation age of the eclogite protolith in Xiarihamu ranges from 886 to 701 Ma, and the age in Langmuri from 925 to 910 Ma, both of which belong to the Tonian period of the Neoproterozoic. Combined with the ages of Dulan and Wenquan eclogite from the neighboring Langmuli areas (828 and 934 Ma, respectively; [17,81]), it can be inferred that the protolith of East Kunlun eclogite was also formed in the Neoproterozoic (likely 925 to 701 Ma). From a geochronological perspective, this period was characterized by the breakup environment of the Rodinia supercontinent [73–75].

Eclogite-normalized REE distribution patterns (Figure 5a) have a right-side-inclined pattern with weakly enriched LREEs. The LREE-enriched eclogite is widely distributed in East Kunlun and on the northern margin of the Qaidam Basin [12,82,83]. In contrast, normalized REE curves of eclogite from Xiarihamu and Langmuri are relatively flat. This type of eclogite protolith may have been formed in a continental rift environment [12,83]. The notable REE enrichment of samples GS2 and GS5 may be related to the contamination by continental crust [84]. The normalized REE distribution pattern of samples GS3 and GS6 also has a left-inclined pattern with LREE depletion, which is similar to that of eclogite found in the Wenquan area in the eastern part of East Kunlun. This type of eclogite protolith with characteristic LREE depletion may have formed in a continental margin environment [17].

The peak metamorphic age of the Langmuri eclogite is  $449.1 \pm 8.5$  Ma, and that of the Xiarihamu eclogite is  $415.6 \pm 2.7$  Ma. The corresponding ages of Langmuri and Xiarihamu mafic-ultramafic rocks are  $438.8 \pm 2.6$  Ma [38] and 423–393 Ma [19,20,23,37], respectively. Thus, the ages of the eclogites and ultramafic rocks in Langmuri eclogite in the eastern part of East Kunlun are apparently older than the ages of Xiarihamu in the western part. Yin and Zhang [25,85] considered that the East Kunlun orogenic belt is a non-Wilson cycle, because most of the collision is oblique, and its junction has a process of collision from point to line to plane, as it spreads from east to west. Therefore, the early Paleozoic collision belt in East Kunlun started from the eastern segment of East Kunlun. The peak metamorphic age of eclogite in East Kunlun is 449–415 Ma, which was in a collision-compression environment and lasted until a post-collisional-extension environment. From the definition of eclogite [86], we know that the formation environment of eclogite successively experienced the compressional environment of subduction-related collision (prograde metamorphism) and extensional environment of post-collision (retrograde metamorphism). In summary, we believe that the eclogite protolith in East Kunlun was formed in the continental-margin-related rift environment. Eclogite was formed in the continental collisional environment, followed by exhumation to the surface in the post-collisional environment.

### 6.3. Role of Eclogite in Metallogeny

The majority of the scholars [19,21,22,37,38] generally believe that the upwelling of mantle-derived magma triggered by orogenesis played a key role in the formation of the Xiarihamu and Langmugri Cu-Ni deposits. However, there are still some doubts about the mechanism of sulfur saturation and sulfide dissolution.

Above, it has been described in the introduction that the eclogites and Cu-Ni deposits in East Kunlun are highly coupled in spatial distribution. Through the study of chronology, it is found that the ages of eclogites and mafic-ultrabasic rocks are close to each other. The peak metamorphic ages of Langmuri and Xiarihamu eclogites are  $449.1 \pm 8.5$  Ma and  $415.6 \pm 2.7$  Ma, respectively, and the ages of Langmuri and Xiarihamu mafic-ultramafic rocks are  $438.8 \pm 2.6$  Ma [38] and 423–393 Ma [19,20,23,37], respectively. The 393 Ma age of Xiarihamu is the youngest, which is the age of banded gabbro with the latest crystallization differentiation of mafic-ultramafic complex [37], and the diagenetic age of ore-bearing pyroxenite is usually 400–423 Ma. In particular, Zhang et al. [11] obtained that the retrograde metamorphic age of the Xiarihamu III eclogite was 409 Ma, which is consistent with the Re-Os isotopic isochron date of 408 Ma for the massive chalcopyrite in this area [23]. In addition, the eclogites and ore-bearing mafic-ultrabasic rocks are very similar in terms of both their normalized REE distribution curves (Figure 5a) and their trace element spider diagrams (Figure 5b). Researchers [87,88] use the similarity of the REE and trace element characteristics as an important criterion for judging whether two rocks are cognate. The similar characteristics of the REEs and trace elements of the eclogites and the ore-bearing mafic-ultrabasic rocks may indicate that eclogite has some internal relationship with mineralization.

Duan et al. [89] studied and analyzed the interstitial amphibole of ore-mineral-bearing rocks (including feldspar harzburgite) from the Xiarihamu area. Their results revealed that core amphibole grains have high contents of  $\text{TiO}_2$ ,  $\text{MgO}$ , and  $\text{Al}_2\text{O}_3$  and low content of  $\text{SiO}_2$ . It shows that the parental magma was suitable for the enrichment of ore-forming materials, and it is considered that the injection of homologous high-magnesium basaltic magma in the later stages leads to the saturation of sulfur and the continuous melting away of sulfide. Wang et al. [19] conducted a sulfur isotopic study on sulfides in different parts of the I and II-1 rock masses and different types of ores in Xiarihamu. The research shows that  $\delta^{34}\text{S}$  contents range from +2.7‰ to +6.1‰, and the sulfur isotopic compositions of different rocks, minerals, and mineralization types are essentially consistent. It is considered that the sulfur may have been saturated in the deep magma chamber. In Xiarihamu, the  $\Sigma\text{PGE}$  ranges from 0.52 ppb to 19.76 ppb, and the PGE content of ores is significantly higher than that of rocks, which may indicate that the ore-forming parent rock experienced sulfur saturation and deep melting, and deep melting may be the main reason for the loss of PGE in parent magma [19,90].

Previous studies have shown that eclogites in the East Kunlun area are products of continental collision [10,12,16,17]. The process of continental subduction often has the complex exchange and circulation of crust–mantle materials [63,91–94], and the interaction of crust mantle materials primarily occurs in subduction zones. Zheng and Chen [94] defined the free space between the descending and overriding plates on the edge of the subduction plate converging boundary, and the interface where material movement occurs as a subduction channel.

When the continental plate is subducted to the mantle level depths, the crustal material scraped by subduction mixes with the peridotite fragments scraped from the bottom of the mantle wedge. They have undergone different degrees of metamorphism, deformation, and even local anatexis, forming different types of HP-UHP metamorphic melanges, or the enriched mantle was formed by metasomatism between the crust and the mantle (Figure 8a, Zheng and Chen [94]). At the same time, some rocks retreat along the subduction channel during continental plate subduction, forming metamorphic rocks of different grades in the subduction zone. The requirement for rocks to retreat from the continental subduction channel is the weakening and detachment of the middle and upper part of the crust [94].

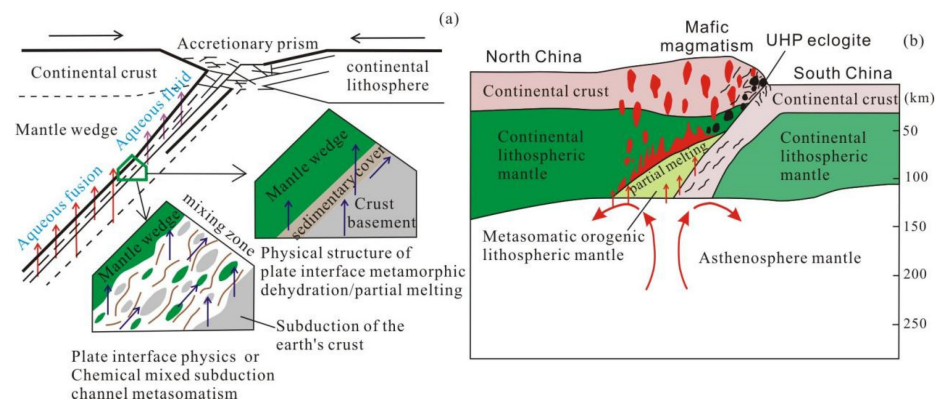


**Figure 8.** (a). The slab–mantle interface in continental subduction channel (Zheng and Chen [94]), and (b) mafic magmatism after continental subduction collision (Zhao et al. [92]) schematic diagram.

In the post-collision stage, the melanges or enriched mantles partially melted under the influence of thermal events, forming various mafic–ultramafic magmas (Figure 8b) [92–94], and these magmas also intruded along the weak zones where the continental crust exhumed in the subduction channel. Because these types of melanges or enriched mantles contain a large amount of input crust material, sulfur saturation may be achieved once partial melting occurs, which can reasonably explain why the metallogenic parent rocks experienced sulfur saturation and sulfide liquation in the deep magma chamber. At the same time, it can also explain the coupling of the spatial distribution of Cu-Ni deposits and eclogites in East Kunlun.

In conclusion, it can be inferred that the formation mechanism of the magmatic liquation type Cu-Ni deposits from East Kunlun is as follows: Deep subduction of continental crust occurred successively in the east and west sections of East Kunlun at the end of the Early Paleozoic (449–415 Ma), and extensive crust-mantle mixing and metasomatism occurred in the subduction zone, resulting in the formation of UHP metamorphic melange or enriched mantle. In the post-collisional extension environment, the subduction plate reached the critical condition, detachment and exhumation occurred, and the metamorphic melange or enriched mantle partially melted due to the asthenospheric thermal effect, forming the sulfur-rich parent magma. The parent magma was deeply liquated in the magma chamber to form ore-bearing magma, which was emplaced along the weak zone (North KunLun fault system) in the subduction tunnel. Sulfide continued to liquate during this period, and a small amount of crustal sulfur was added to form the Cu-Ni deposits. At the same time, part of the mafic magma continued to be emplaced along the subduction channel and was in place near the central Kunlun fault system (Figure 9).

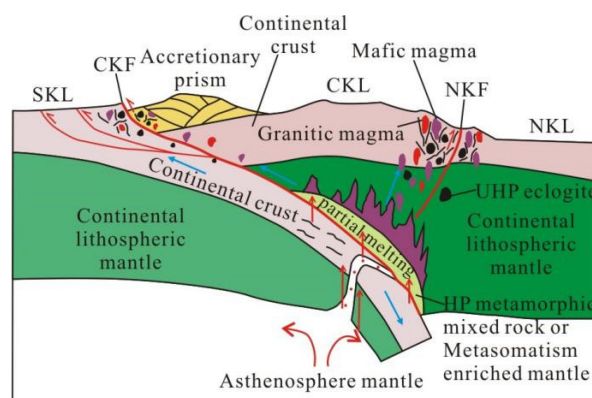


**Figure 9.** The formation mechanism diagram of magmatic liquation type Cu-Ni ore in East Kunlun orogenic belt. SKL—South Kunlun; CKL—Central Kunlun; NKL—North Kunlun; CKF—Central Kunlun fault; NKF—North Kunlun fault.

## 7. Conclusions

(1) The peak metamorphic age of the Xiarihamu eclogite is  $415.6 \pm 2.7$  Ma (MSWD = 0.43,  $n = 16$ ), and the peak metamorphic age of the Langmuri eclogite is  $449.1 \pm 8.5$  Ma (MSWD = 0.88,  $n = 19$ ). The peak metamorphic ages (retrograde metamorphic ages) of eclogite are older or essentially the same as that of mafic-ultramafic intrusion of the magmatic liquation-type Cu-Ni deposit.

(2) Eclogites from the Xiarihamu and Langmuri have  $\text{SiO}_2$  contents of 47.56 wt.% to 52.32 wt.% and  $\text{Mg}^\#$  values of 41.9 to 61.24. The normalized REE distribution patterns showed overall characteristics of inclination towards the right side or a flat type of distribution due to weak LREE enrichment, weak negative Eu anomalies, relative enrichment in LILEs such as K and Rb, depletion in HFSEs such as Nb and Zr, and V-shaped valleys caused by depletions in P and Ti. It has the characteristics of E-MORB-type basalt and was formed in the continental collision environment after the closure of the Proto-Tethys.

(3) The deep subduction of the continent brought a large amount of sulfur from the crust into the mantle, which is the key process to cause the mineralization of the East Kunlun magmatic liquation type Cu-Ni deposits in the post-collisional extensional environment. At the same time, the eclogite exhumation and the intrusion emplacement of mafic-ultramafite may have used the subduction channel together, which may have resulted in the coupling relationship between eclogites and Cu-Ni deposits in the East Kunlun area.

**Supplementary Materials:** Supplementary data to this article can be found at <https://www.mdpi.com/article/10.3390/min13030330/s1>: Table S1. LA-ICP-MS U-Th-Pb isotopic analyses of zircon from the eclogite in Xiarihamu and Langmuri areas, East Kunlun.

**Author Contributions:** Conceptualization, T.P. and A.Z.; methodology, A.Z. and Y.Z.; software, Y.Q.; investigation, Y.B.; resources, Y.Q.; data curation, S.H.; writing—original draft preparation, Y.Z.; visualization, Y.Z.; project administration, A.Z.; funding acquisition, T.P. All authors have read and agreed to the published version of the manuscript.

**Funding:** This research was financially supported by Kunlun Talent of Qinghai Province, China (QRCZ2020-18, QDKK2021-61), National Natural Science Foundation of China (2019QZKK0806, 92062217), and Technology Department Foundation of Qinghai Province, China (2019-ZJ-7009).

**Data Availability Statement:** Data are available in the article or Supplementary Materials.

**Acknowledgments:** Thanks for the great effort by editors and reviewers.

**Conflicts of Interest:** The authors declare no conflict of interest.

## References

1. Liu, Y.X.; Tang, H.S.; Wu, H.Z. Types and ore-control factors of Cu-Ni sulfide deposits in China. *Miner. Resour. Geol.* **1998**, *64*, 86–90.
2. Li, X.H.; Su, L.; Chung, S.L.; Li, Z.X.; Liu, Y.; Song, B.; Liu, D.Y. Formation of the Jinchuan ultramafic intrusion and the world's third largest Ni-Cu sulfide deposit: Associated with the 825 Ma south China mantle plume? *Geochem. Geophys. Geosyst.* **2005**, *6*, 1–16. [[CrossRef](#)]
3. Tang, Z.L.; Yan, H.Q.; Jiao, J.G.; Pan, Z.X. Regional metallogenic controls of small-intrusion-hosted Ni-Cu(PGE) ore deposits in China. *Earth Sci. Front.* **2007**, *14*, 92–103. [[CrossRef](#)]
4. Liu, Y.G.; Li, W.Y.; Jia, Q.Z.; Zhang, Z.W.; Wang, Z.A.; Zhang, Z.B.; Zhang, J.W.; Qian, B. The dynamic sulfide saturation process and a possible slab break-off model for the giant Xiarihamu magmatic nickel ore deposit in the East Kunlun orogenic belt, northern Qinghai-Tibet plateau, China. *Econ. Geol.* **2018**, *113*, 1383–1417. [[CrossRef](#)]
5. Zhou, W.; Wang, B.Y.; Xia, M.Z.; Xia, Z.D.; Jiang, C.Y.; Dong, J.; Xie, E.S. Mineralogical characteristics of Shitoukengde mafic-ultramafic intrusion and analysis of its metallogenic potential, East Kunlun. *Acta Petrol. Mineral.* **2016**, *35*, 86–96.
6. Zhang, Z.W.; Wang, Y.L.; Qian, B.; Liu, Y.G.; Qi, C.W.; Dong, J.; Yin, J.H. Mineralogical characteristics of the shitoukengde mafic-ultramafic intrusions in East Kunlun orogenic belt and the ore-forming indication. *Geol. Explor.* **2017**, *53*, 825–837.
7. Shi, G.H.; Xiong, S.Y.; Li, Y.N.; Wang, Y.; Zhang, L.B. Analysis on prospecting potential of Langmuri Nickel polymetallic deposit in East Kunlun orogenic belt, Qinghai. *Miner. Explor.* **2018**, *54*, 1205–1211.
8. Jia, L.H. *Genesis of the Wenquan Ultramafic Rocks in East Kunlun Orogen, Northwest China*; China University of Geosciences: Beijing, China, 2015; pp. 21–54.

9. Kong, H.L.; Li, J.C.; Guo, X.Z.; Yao, X.G.; Jia, Q.Z. The discovery of Early Devonian pyroxene peridotite from the Xiwanggou magmatic Ni-Cu sulfide ore spot in East Kunlun Mountains. *Geol. China* **2019**, *46*, 205–206.
10. Qi, S.S.; Song, S.G.; Shi, L.C.; Cai, H.J.; Hu, J.C. Discovery and its geological significance of Early Paleozoic eclogite in Xiarihamu-Suhaitu area, western part of the East Kunlun. *Acta Petrol. Sin.* **2014**, *30*, 3345–3356.
11. Zhang, Z.W.; Qian, B.; Li, W.Y.; Wang, Y.L.; Zhang, J.W.; You, M.X.; Liu, Y.G. The discovery of Early Paleozoic eclogite from the Xiarihamu magmatic Ni-Cu sulfide deposit in eastern Kunlun orogenic belt: Zircon U-Pb chronologic evidence. *Geol. China* **2017**, *44*, 816–817.
12. Fan, Y.Z.; Meng, F.C.; Duan, X.P. The protoliths of the xiarihamu eclogites from the western part of east Kunlun and continent/arc-continent collision. *Acta Geol. Sin.* **2018**, *92*, 482–502.
13. Du, W.; Jiang, C.Y.; Tang, Z.L.; Xia, M.Z.; Xia, Z.D.; Ling, J.L.; Zhou, W.; Wang, B.Y. Discovery of the Dagele Eclogite in East Kunlun, Western China and Its Zircon SHRIMP U-Pb Ages: New Constrains on the Central Kunlun Suture Zone. *Acta Geol. Sin.* **2017**, *91*, 1153–1154. [[CrossRef](#)]
14. Guo, X.Z.; Jia, Q.Z.; Li, J.C.; Kong, H.L.; Yao, X.G.; Mi, J.R.; Qian, B.; Wang, Y. Zircon U-Pb geochronology and geochemistry and their geological significances of eclogites from east Kunlun high-pressure metamorphic belt. *Earth Sci.* **2018**, *43*, 4300–4318.
15. Qi, X.P.; Fan, X.G.; Yang, J.; Cui, J.T.; Wang, B.Y.; Fan, Y.Z.; Yang, G.X.; Li, Z.; Chao, W.D. The discovery of Early Paleozoic eclogite in the upper reaches of Langmuri in eastern East Kunlun Mountains and its significance. *Geol. Bull. China* **2016**, *35*, 1771–1783.
16. Meng, F.C.; Zhang, J.X.; Cui, M.H. The Discovery of Early Paleozoic eclogite from the East Kunlun, western China and its tectonic significance. *Gondwana Res.* **2013**, *23*, 825–836. [[CrossRef](#)]
17. Meng, F.C.; Cui, M.H.; Jia, L.H.; Ren, Y.F.; Feng, H.B. Paleozoic continental collision of the East Kunlun orogen: Evidence from protoliths of the eclogites. *Acta Petrol. Sin.* **2015**, *31*, 3581–3594.
18. Ma, C.Q.; Xiong, F.H.; Zhang, J.Y.; Liu, B.; Huang, J.; Jiang, H.A. Influence of subduction plate on magmatism from plate subduction to post-orogenic stage: Evidence from Early Permian to Late Triassic mafic dyke group in East Kunlun. *Acta Geol. Sin.* **2013**, *87*, 79–81.
19. Wang, G.; Sun, F.Y.; Li, B.L.; Li, S.J.; Zhao, J.W.; Ao, C.; Yang, Q.A. Petrography, zircon U-Pb geochronology and geochemistry of the mafic-ultramafic intrusion in Xiarihamu Cu-Ni deposit from East Kunlun, with implications for geodynamic setting. *Geosci. Front.* **2014**, *21*, 381–401. [[CrossRef](#)]
20. Zhang, Z.W.; Li, W.Y.; Qian, B.; Wang, Y.L.; Li, S.J.; Liu, C.Z.; Zhang, J.W.; Yang, Q.A.; You, M.X.; Wang, Z.A. Metallogenic epoch of the Xiarihamu magmatic Ni-Cu sulfide deposit in eastern Kunlun orogenic belt and its prospecting significance. *Geol. China* **2015**, *42*, 438–451.
21. Pan, T. The prospecting for magmatic liquation type nickel deposits on the southern and northern margin of Qaidam Basin, Qinghai Province: A case study of the Xiarihamu Ni-Cu sulfide deposit. *Geol. China* **2015**, *42*, 713–723.
22. Pan, T.; Li, S.P.; Zhao, C.X.; Chen, J.; Jin, T.T.; Lin, H. Metallogenic model and prospecting direction of the Xiarihamu Ni-Cu sulfide deposit in East Kunlun area. *Geol. Bull. China* **2017**, *36*, 1276–1287.
23. Li, H.R.; Qian, Y.; Sun, F.Y.; Sun, J.L.; Wang, G. Zircon U-Pb dating and sulfide Re-Os isotopes of the Xiarihamu Cu-Ni sulfide deposit in Qinghai Province, Northwestern China. *Can. J. Earth Sci.* **2020**, *57*, 885–902. [[CrossRef](#)]
24. Ren, J.S. The continental tectonics of China. *Bull. Chin. Acad. Geol. Sci.* **1994**, *Z2*, 5–13. [[CrossRef](#)]
25. Yin, H.F.; Zhang, K.X. Characteristics of the eastern Kunlun orogenic belt. *Earth Sci. J. China Univ. Geosci.* **1997**, *22*, 339–342.
26. Jiang, C.F.; Wang, Z.Q.; Li, J.T. *Opening and Closing Tectonics of the Central Asian Orogenic Belt*; Geological Publishing House: Beijing, China, 2000; pp. 1–107.
27. Xu, Z.Q.; Yang, J.S.; Li, H.B.; Zhang, J.X.; Zeng, L.L.; Jiang, M. The Qinghai-Tibet plateau and continental dynamics: A review on terrain tectonics, collisional orogenesis, and processes and mechanisms for the rise of the plateau. *Geol. China* **2006**, *33*, 221–238.
28. Xu, W.Y.; Zhang, D.Q.; Yan, S.H.; Li, D.X.; Feng, C.Y.; She, H.Q.; Dong, Y.J. Advances and prospecting of the mineral resources survey in Eastern Kunlun Area. *Geol. China* **2001**, *28*, 25–29.
29. Li, Z.M.; Xue, C.J.; Wang, X.H.; Tang, H.; Tu, Q.J.; Teng, J.X.; Li, R.S. Features of regional mineralization and analysis of the exploration development in the Eastern Kunlun mountains. *Geol. Rev.* **2007**, *53*, 708–718.
30. Pan, T.; Bai, Y.S.; Sun, F.Y.; Chen, J.P. *Metallogenic Series of East Kunlun Nonferrous and Precious Metal Ores in Qinghai Province*; Geological Publishing House: Beijing, China, 2011; pp. 1–250.
31. Pan, T. Classification of metallogenic units in Qinghai, China. *J. Earth Sci. Environ.* **2017**, *39*, 16–33.
32. Yuan, W.M.; Mo, X.X.; Yu, X.H.; Luo, Z.H. The Record of Indosinian Tectonic Setting from the Granotoid of Eastern Kunlun Mountains. *Geol. Rev.* **2000**, *46*, 203–211.
33. Mo, X.X.; Luo, Z.H.; Deng, J.F.; Yu, X.H.; Liu, C.D.; Shen, H.W.; Yuan, W.M.; Liu, Y.H. Granitoids and Crustal Growth in the East-Kunlun Orogenic Belt. *Geol. J. China Univ.* **2007**, *13*, 403–414.
34. Pan, T. Discussion on ore controlling condition of Dulengou Cu-Co deposit in Eastern Kunlun metallogenic belt, Qinhai. *Miner. Resour. Geol.* **2004**, *18*, 109–112.
35. Pan, T. Geochemical features and origin of siliceous rocks of Kendekeke Co-Au deposit in the eastern Kunlun metallogenic belt, Qinhai. *Geol. Prospect.* **2008**, *44*, 51–54.
36. Pan, T. Discussion on the Minerogenetic Series of Deposits in Qinghai, China. *J. Earth Sci. Environ.* **2019**, *41*, 297–315.

37. Li, S.J.; Sun, F.Y.; Gao, Y.W.; Zhao, J.W.; Li, L.S.; Yang, Q.A. The theoretical guidance and the practice of small intrusions forming large deposits—The enlightenment and significance for searching breakthrough of Cu-Ni sulfide deposit in Xiarihamu, East Kunlun, Qinghai. *Northwestern Geol.* **2012**, *45*, 185–191.
38. Meng, Q.P. *Study on Geological Characteristics and Genesis of Langmuri Copper-Nickel Deposit in Eastern Kunlun, Qinghai*; Jilin University: Changchun, China, 2019; pp. 1–86.
39. Ao, C.; Sun, F.Y.; Li, B.L.; Li, S.J.; Wang, G. Geochemistry, zircon U-Pb dating and geological significance of diorite porphyrite in Xiarihamu deposit, eastern Kunlun orogenic belt, Qinghai. *Northwestern Geol.* **2014**, *47*, 96–106.
40. Yang, S.Y.; Jiang, S.Y.; Mao, Q.; Chen, Z.Y.; Rao, C.; Li, X.L.; Li, W.C.; Yang, W.Q.; He, P.L.; Li, X. Electron probe microanalysis in geosciences: Analytical procedures and recent advances. *At. Spectrosc.* **2022**, *43*, 186–200. [[CrossRef](#)]
41. Hou, K.J.; Li, Y.H.; Tian, Y.R. In situ U-Pb zircon dating using laser ablation-multi ion counting-ICP-MS. *Miner. Depos.* **2009**, *28*, 481–492.
42. Winchester, J.A.; Floyd, P.A. Geochemical discrimination of different magma series and their differentiation products using immobile elements. *Chem. Geol.* **1977**, *20*, 325–343. [[CrossRef](#)]
43. Muller, D.; Groves, D.I. *Potassic Igneous Rocks and Associated Gold- Copper Mineralization*; Springer: Berlin, Germany, 1995; pp. 1–144.
44. Taylor, S.R.; McLennan, S.M. *The Continental Crust: Its Composition and Evolution*; Blackwell Scientific Publication: London, UK, 1985; p. 312.
45. Sun, S.S.; McDonough, W.F. Chemical and isotopic systematics of oceanic basalts: Implications for mantle composition and processes. *Geol. Soc. Lond. Spec. Publ.* **1989**, *42*, 313–345. [[CrossRef](#)]
46. Taylor, S.R.; McLennan, S.M. The composition and evolution of the continental crust: Rare earth element evidence from sedimentary rocks. *Philos. Trans. R. Soc. A* **1981**, *301*, 381–399.
47. Turekian, K.K.; Wedepohl, K.H. Distribution of the elements in some major units of the earth's crust. *Geol. Soc. Am. Bull.* **1961**, *72*, 175–192. [[CrossRef](#)]
48. Cong, B.L.; Zhang, W.H. Garnet of eclogite. *Chin. Sci. Bull.* **1977**, *9*, 413–416.
49. Coleman, R.G.; Lee, D.E.; Beatty, L.B.; Brannock, W.W. Eclogites and eclogites: Their differences and similarities. *Geological Soc. Am. Bull.* **1965**, *76*, 483–508. [[CrossRef](#)]
50. Lei, W.Y.; Shi, G.H.; Liu, Y.X. Research progress on trace element characteristics of zircons of different origins. *Earth Sci. Front.* **2013**, *20*, 273–284.
51. Mahdy, N.M.; Baher, A.; El Kalioubi, B.A.; Wohlgemuth-Ueberwasser, C.C.; Shalaby, M.H.; El-Afandy, A.H. Petrogenesis of U- and Mo-bearing A2-type granite of the Gattar batholith in the Arabian Nubian Shield, Northeastern Desert, Egypt: Evidence for the favorability of host rocks for the origin of associated ore deposits. *Ore Geol. Rev.* **2015**, *75*, 57–81. [[CrossRef](#)]
52. Mahdy, N.M. Textural and chemical characteristics of zircon, monazite, and thorite, Wadi Al-Baroud area, Eastern Desert of Egypt: Implication for rare metal pegmatite genesis. *Ore Geol. Rev.* **2021**, *136*, 104225. [[CrossRef](#)]
53. Belousova, E.A.; Griffin, W.L.; O'Reilly, S.Y.; Fisher, N.I. Igneous zircon: Trace element composition as an indicator of source rock type. *Contrib. Mineral. Petrol.* **2002**, *143*, 602–622. [[CrossRef](#)]
54. Guo, X.; Yan, Z.; Fu, C.; Wang, Z. Formation age and tectonic attribute of jinshuikou group complex in the Nanshan area, Qinghai. *Acta Geol. Sin.* **2016**, *90*, 589–606.
55. Lu, S.N.; Li, H.C.; Wang, H.C.; Chen, Z.H.; Zheng, J.K.; Xiao, Z.Q. Detrital zircon population of Proterozoic meta-sedimentary strata in the Qinling-Qilian-Kunlun Orogen. *Acta Petrol. Sin.* **2009**, *25*, 2195–2208.
56. Li, M.; Zha, X.F.; Hu, C.B.; Gao, X.F.; Li, T.; Yao, Z.L. Zircon U-Pb geochronology of the Baishahe Formation in the western part of East Kunlun Orogenic Belt: Constraints on Precambrian basement evolution. *Geol. Bull. China* **2021**, *40*, 41–57.
57. Wetherill, G.W. Discordant uranium-lead ages. *Trans. Am. Geophys. Union* **1956**, *37*, 320–326. [[CrossRef](#)]
58. Hoskin, P.W.O.; Black, L.P. Metamorphic zircon formation by solid-state recrystallization of protolith igneous zircon. *Meta-morphic Geol.* **2000**, *18*, 423–439. [[CrossRef](#)]
59. Geisler, T.; Ulonska, M.; Schleicher, H.; Pidgeon, R.T.; Bronswijk, W.V. Leaching and differential recrystallization of metamict zircon under experimental hydrothermal condition. *Contrib. Miner. Pet.* **2001**, *141*, 53–65. [[CrossRef](#)]
60. Zhang, Y.Q. Effect of radiogenic lead loss in zircon on in-situ U-Pb dating and data correction method. *J. Geol.* **2015**, *89*, 62–63.
61. Bernard, G.J.; Cornichet, J. Origin of eclogites from South Brittany, France: A Sm-Nd isotopic and REE study. *Chem. Geol. Isot. Geosci. Sect.* **1985**, *52*, 185–201. [[CrossRef](#)]
62. Jahn, B.M.; Rumble, D.; Liou, J.G. Geochemistry and isotope tracer study of UHP metamorphic rocks // Ultrahigh Pressure Metamorphism. *EMU Notes Mineral.* **2003**, *32*, 365–414.
63. Zheng, Y.F. Metamorphic chemical geodynamics in continental subduction zones. *Chem. Geol.* **2012**, *328*, 5–48. [[CrossRef](#)]
64. Wang, H.; Wu, Y.B.; Gao, S.; Liu, X.C.; Liu, Q.; Qin, Z.W.; Xie, S.W.; Zhou, L.; Yang, S.H. Continental origin of eclogites in the North Qinling terrane and its tectonic implications. *Precambrian Res.* **2013**, *230*, 13–30. [[CrossRef](#)]
65. Dong, Y.H.; Wang, Q.; Xu, J.F.; Zi, F. Dongyue Lake adakitic volcanic rocks with high Mg<sup>#</sup> in north Qiangtang block: Petrogenesis and its tectonic implication. *Acta Petrol. Sin.* **2008**, *24*, 291–302.
66. Niu, Y.N. Generation and evolution of basaltic magmas: Some basic concepts and a new view on the origin of mesozoic-cenozoic basaltic volcanism in Eastern China. *Geol. J. China Univ.* **2005**, *11*, 9–46.
67. Vervoot, J.D.; Pachel, P.J.; Gehres, G.; Nutman, A.P. Constraints on early Earth differentiation from Hafnium and Neodymium isotopes. *Nature* **1996**, *379*, 624–627. [[CrossRef](#)]

68. Fan, J.T.; Cheng, Z.X. HP-UHP metamorphism and deformation in Northern Jiangsu and its metallogeny. *Geotecton. Metallog.* **1998**, *22*, 65–74.
69. Lu, S.N. *Preliminary Study on Precambrian Geology in the Northern Qinghai-Tibet Plateau*; Geological Publishing House: Beijing, China, 2002; pp. 1–125.
70. Wang, G.C.; Wang, Q.H.; Jian, P.; Zhu, Y.H. Zircon SHRIMP ages of Precambrian metamorphic basement rocks and their tectonic significance in the eastern Kunlun Mountains, Qinghai Province, China. *Geosci. Front.* **2004**, *11*, 481–490.
71. Condie, K.C. Continent grouping during formation of Rodinia at 1.35–0.9Ga. *Gondwana Res.* **2001**, *4*, 5–16. [[CrossRef](#)]
72. Chen, Y.X.; Pei, X.Z.; Li, Z.C.; Li, R.B.; Liu, C.J.; Chen, G.C.; Pei, L.; Wei, B. Geochronology, geochemical features and geological significance of the granitic gneiss in Balong area, East Section of East Kunlun. *Acta Petrol. Sin.* **2015**, *31*, 2230–2244.
73. Lu, S.N. A Review of Advance in the Research on the Neoproterozoic Rodinia Supercontinent. *Geol. Rev.* **1998**, *44*, 489–495.
74. Lu, S.N. From Rodinia to Gondwanaland Supercontinents—Thinking about problems of researching neoproterozoic supercontinents. *Earth Sci. Front.* **2001**, *8*, 441–448.
75. Ren, J.H.; Zhang, K.; Liu, Y.Q.; Zhou, D.W.; Feng, Q. Geochemical characteristics and zircon dating of blasto-gabbro from the South Jinshuikou area, Eastern Kunlun. *Journal of Northwest University.* **2011**, *41*, 100–106.
76. Yang, J.S.; Robinson, P.T.; Jiang, C.F.; Xu, Z.Q. Ophiolites of the Kunlun Mountains. China and their tectonic implications. *Tectonophysics* **1996**, *258*, 215–231. [[CrossRef](#)]
77. Li, H.K.; Lu, S.N.; Xiang, Z.Q.; Zhou, H.Y.; Guo, H.; Song, B.; Zheng, J.K.; Gu, Y. SHRIMP U-Pb zircon age of the granulite from the Qingshuiquan area, Central Eastern Kunlun Suture Zone. *Arth Sci. Front.* **2006**, *13*, 311–321.
78. Zhang, Y.F.; Pei, X.Z.; Ding, S.P.; Li, R.B.; Feng, J.B.; Sun, Y.; Li, Z.C.; Chen, Y.; Chen, Y.X. LA-ICP-MS zircon U-Pb age of quartz diorite at the Kekesha area of Dulan County, eastern section of the East Kunlun orogenic belt, China and its significance. *Geol. Bull. China* **2010**, *29*, 79–85.
79. Liu, B.; Ma, C.Q.; Zhang, J.Y.; Xiong, F.H.; Huang, J.; Jiang, H.A. Petrogenesis of Early Devonian intrusive rocks in the east part of Eastern Kunlun Orogen and implication for Early Palaeozoic orogenic processes. *Acta Petrol. Sin.* **2012**, *28*, 1785–1807.
80. Zhao, Z.M.; Ma, H.D.; Wang, B.Z.; Bai, Y.S.; Li, R.S.; Ji, W.H. The evidence of intrusive rocks about collision-orogeny during early devonian in Eastern Kunlun Area. *Geol. Rev.* **2008**, *54*, 1–11.
81. Yu, S.Y.; Zhang, J.X.; Li, H.K.; Hou, K.J.; Mattinson, C.G.; Gong, J.H. Geochemistry, zircon U-Pb geochronology and Lu-Hf isotopic composition of eclogites and their host gneisses in the Dulan area, North Qaidam UHP terrane: New evidence for deep continental subduction. *Gondwana Res.* **2013**, *23*, 901–919. [[CrossRef](#)]
82. Amelin, Y.; Lee, D.C.; Halliday, A. Early-middle Archaean crustal evolution deduced from Lu-Hf and U-Pb isotopic studies of single zircon grains. *Geochim. Cosmochim. Acta* **2000**, *64*, 4205–4225. [[CrossRef](#)]
83. Zhang, C.; Zhang, L.F.; Bader, T.; Song, S.G.; Lou, Y.X. Geochemistry and trace element behaviors of eclogite during its exhumation in the Xitieshan terrane, North Qaidam UHP belt, NW China. *J. Asian Earth Sci.* **2013**, *63*, 81–97. [[CrossRef](#)]
84. Bai, Y.; Guo, Z.P.; Zhao, X.M. Geochronology, Hf isotopic and geochemical characteristics of Maozang granodiorite in Langlike area, North Qilian Mountain. *Miner. Depos.* **2017**, *36*, 158–170.
85. Yin, H.F.; Zhang, K.X. Evolution and Characteristics of the central orogenic belt. *Earth Sci. J. China Univ. Geosci.* **1998**, *23*, 437–442.
86. Carswell, D.A.; Harley, S.I. *Mineral Barometry and Thermometry//Carswell D A. Eclogite Facies Rocks*; Chapman and Hall: New York, NY, USA, 1990; pp. 83–110.
87. Lu, C.Z.; Yan, T.Z.; Dong, C.W.; Gu, M.G. Magmatic consanguinity analysis of the Muchen intrusion and Xishantou Formation volcanic rocks in Zhejiang. *Geol. China* **2006**, *33*, 146–152.
88. Wang, M.; Li, C.; Zhai, Q.G.; Xie, C.M.; Wu, Y.W. Magma homology of mafic dyke and basalt in southern Qiangtang, northern Tibet, China. *Geol. Bull. China* **2009**, *28*, 1281–1289.
89. Duan, X.P.; Meng, F.C.; Fan, Y.Z. The constraints of kaersutite and pargasite on metallogeny in Xiarihamu mafic-ultramafic intrusion, East Kunlun. *Acta Petrol. Sin.* **2019**, *35*, 1819–1832.
90. Du, W.; Ling, J.L.; Zhou, W.; Wang, Z.X.; Xia, Z.D.; Xia, M.Z.; Fan, Y.Z.; Jiang, C.Y. Geological characteristics and genesis of Xiarihamu nickel deposit in East Kunlun. *Miner. Depos.* **2014**, *33*, 713–726.
91. Zhao, Z.F.; Zheng, Y.F.; Zhang, J.; Dai, L.Q.; Li, Q.; Liu, X. Syn-exhumation magmatism during continental collision: Evidence from alkaline intrusives of Triassic age in the Sulu orogen. *Chem. Geol.* **2012**, *328*, 70–88. [[CrossRef](#)]
92. Zhao, Z.F.; Dai, L.Q.; Zheng, Y.F. Postcollisional mafic magmatism records the crust-mantle interaction of continental subduction-zone. *Chin. Sci. Bull.* **2013**, *58*, 2310–2315.
93. Zheng, Y.F.; Zhao, Z.F.; Chen, Y.X. Continental subduction channel processes: Plate interface interaction during continental collision. *Chin. Sci. Bull.* **2013**, *58*, 2233–2239. [[CrossRef](#)]
94. Zheng, Y.F.; Chen, Y.X. Crust-mantle interaction in continental subduction zones. *Earth Sci.* **2019**, *44*, 3961–3983.

**Disclaimer/Publisher’s Note:** The statements, opinions and data contained in all publications are solely those of the individual author(s) and contributor(s) and not of MDPI and/or the editor(s). MDPI and/or the editor(s) disclaim responsibility for any injury to people or property resulting from any ideas, methods, instructions or products referred to in the content.